Residue alkalinity limits microbial leaching of rare earth elements from industrial wastes

Shahram Asgari

Department of Marine Sciences, University of Georgia, Athens, GA 30602, USA

ORCID: 0009-0004-3810-2739

Corresponding author: Shahram Asgari, shahram.asgari@uga.edu

Peer-review status

This manuscript is a non-peer-reviewed preprint submitted to EarthArXiv. It has not yet been submitted to a journal. Later versions of this preprint will note the journal submission and, if accepted, the published DOI.

Preprint version 1, October 2026.

Residue alkalinity limits microbial leaching of rare earth elements from industrial wastes

Shahram Asgari

Department of Marine Sciences, University of Georgia, Athens, GA 30602, USA

Correspondence: Shahram Asgari (shahram.asgari@uga.edu)

Abstract

Microorganisms that make acids can recover rare earth elements from industrial residues such as red mud, coal fly ash, phosphogypsum and electronic waste. Most published studies test one organism on one residue, so their results are hard to transfer. Here we compiled 17 bioleaching studies, covering 10 residues, 5 groups of organisms and 217 runs. We described them all with one physical model, BioLixa. The model links acid production by the organism, the charge balance of the solution and the alkalinity of the residue. From the resulting pH it computes release of the metal from three hosts in the solid and its loss to oxalate precipitation and hydrolysis. A single parameter set, shared by organism group and by residue, was fitted to 13 studies. It reproduced 552 recovery measurements with a mean absolute error of 2.3 percentage points (R^2 = 0.97) and 811 pH measurements with a mean error of 0.54 pH units. The fitted model shows that the alkalinity of the residue often decides whether bioleaching works. Leaching proceeds only when the acid made by the organism exceeds the base capacity of the residue. For red mud, a fungus succeeds only below about 3 % solids. The model also gives, for each residue, the threshold acid dose and the share of rare earths that any acid can reach. For forecasting, BioLixa was the most accurate of eight methods when only the conditions of a run were known, in a development rehearsal and in four held-out studies. Once early recovery points were known, assimilating the early pH as well cut its rehearsal error by 30 % and placed it ahead of all data-driven regressors, although simply holding the last measured value remained hard to beat and the success criterion of the held-out test was not met. BioLixa makes published bioleaching results comparable, explains why runs fail, and gives parameters for designing microbial recovery of rare earths from residues.

Keywords: bioleaching; rare earth elements; critical minerals; industrial residues; red mud; organic acids; charge balance; hierarchical model; pre-registered test

1 Introduction

Rare earth elements go into permanent magnets, phosphors and catalysts, and a few mines supply most of them (U.S. Geological Survey, 2025). Some of the rare earths that industry has already handled end up in residues. Examples are red mud from alumina refining (Borra et al., 2015), coal fly ash (Taggart et al., 2016), phosphogypsum, spent catalysts and lamp phosphors (Binnemans et al., 2013). These residues are already ground, and many are stockpiled. Strong mineral acids can leach them, but they use a lot of reagent and leave an acidic waste.

Bioleaching replaces part of that reagent with acids made by microorganisms. Fungi such as Aspergillus niger and Penicillium excrete citric, gluconic and oxalic acid. Acetic acid bacteria such as Gluconobacter oxydans turn glucose into gluconic acid. Sulfur-oxidising acidophiles such as Acidithiobacillus make sulfuric acid (Gadd, 2010; Barmettler et al., 2016). Organic acids lower the pH and

also bind the released metal (Gadd, 2010). Rare earths have been leached in this way from monazite (Brisson et al., 2016), lamp phosphors and cracking catalysts (Reed et al., 2016), red mud (Qu and Lian, 2013; Pedram et al., 2020), circuit boards (Gonzalez Baez et al., 2024) and coal fly ash (Park and Liang, 2019).

Most of these studies test one organism on one residue under their own conditions. The organism can grow in contact with the residue (one-step), or the residue can be added after the organism has grown for some days (two-step). Other runs use the cell-free culture liquid (spent medium) or a chemical acid as a control. The results are recovery curves, sometimes with pH and acid concentrations over time. In the studies we compiled, these results were analysed one study at a time. Some authors fitted shrinking-core or other kinetic models to each curve (Pedram et al., 2020), and others optimised the conditions with response surfaces (Bahaloo-Horeh and Mousavi, 2022; Gonzalez Baez et al., 2024). Machine learning on compiled data has been tried for chemical leaching (Nguyen et al., 2025), but such models go from conditions to recovery directly. A curve fitted to one study says little about the next residue, and a regression across studies cannot show why a run failed.

The processes between the organism and the recovered metal are known in outline. The organism makes acid at some rate. The residue consumes part of it, since red mud is strongly alkaline and many ashes contain lime. The acid that is left sets the pH and the amount of free organic ligand. These two control how fast the minerals that hold the rare earths dissolve. Some of the released metal is lost again, to oxalate precipitation or to hydrolysis when the pH rises. Each of these processes has been described before. To our knowledge, however, they have not been combined in a single model with parameters shared across studies and fitted to the published data as a whole.

Here we build and test such a model, BioLixa. It follows the chain from organism to acid, pH, release and loss (Fig. 1). Its parameters belong to the organism group, to the residue or to all runs. BioLixa extends two earlier models of chemical leaching. Lixa designs leaching from the pore to the plant scale (Asgari, 2026a), and LixaLearn learns how a new residue leaches from a few laboratory tests (Asgari, 2026b). BioLixa adds the microbial acid supply and the solution chemistry that connect the organism to the residue. We address three questions. Can one parameter set describe recovery and pH across many studies? What does the fitted model say about why bioleaching fails? Can it predict the rest of a new run from its first few points better than models without chemistry? The last question was tested once, on four studies set aside before any model was built.

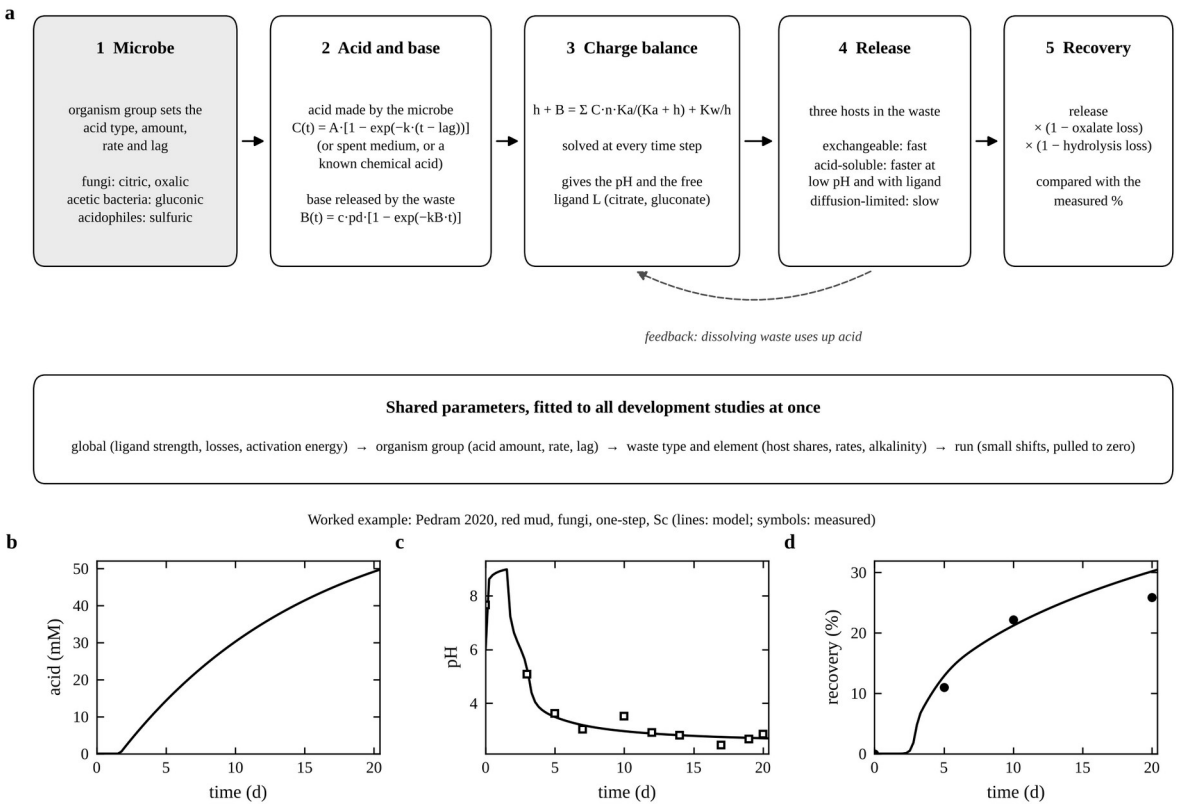


Figure 1. The BioLixa model. (a) The chain from organism to recovery; the dashed arrow is the acid used up by the dissolving residue, which feeds back on the pH. Parameters are shared at four levels (bottom box). (b to d) One fitted development run (Pedram et al., 2020; Aspergillus niger, one-step, red mud, scandium): (b) acid made by the organism, (c) pH, (d) recovery. Lines are the model, symbols are the measurements.

2 Methods

2.1 Data compilation

We searched for studies of rare earth bioleaching from residues and wastes. A study was kept if a microorganism or its culture liquid leached rare earths from a residue and at least one time series was reported. For each study we extracted every rare earth result, the matching pH, organic acid or sulfate data, and the run conditions. These were the organism, mode, solids loading, temperature, starting pH and any acid added. Values in tables and text were copied directly. Points in vector figures were read from the drawing commands of the PDF with PyMuPDF and calibrated against at least two labelled ticks per axis. Their uncertainty is half the marker size or 0.2 % of the axis range, whichever is larger. Raster figures were rendered at 300 dpi or more, and the markers were located in pixels. Their uncertainty is the marker half-width plus one pixel, and at least 1 % of the axis range. Every digitised figure was checked by plotting the extracted points over the original image. Concentrations were converted to recovery only where the paper gave the residue grade and the solids loading.

The runs were then harmonised by fixed rules. Organisms were assigned to groups by genus. Fungi are Aspergillus, Penicillium, Talaromyces and Phanerochaete. Acetic acid bacteria are Gluconobacter, Komagataeibacter, Acetobacter and the Kombucha consortium. Acidophiles are Acidithiobacillus,

Sulfobacillus and Leptospirillum. Yeasts are Candida, Cryptococcus, Zygosaccharomyces and Yarrowia, and other heterotrophs are Pseudomonas, Acinetobacter and Bacillus. Modes were assigned from the run descriptions. Where a run reported several elements, each element formed its own series, with shared pH and acid data. A short list of study-specific rules was also applied, each with its reason. For example, reconstituted acid mixtures were given the concentrations from the paper's own table, and residues added after a growth period were given that addition time. The two residues of Reed et al. (2016) were separated by figure. The code lists all rules. The split into development and held-out studies was written down before any model was built (Sect. 2.6).

2.2 Model

BioLixa links five processes (Fig. 1): acid production by the organism, release of base by the residue, the charge balance that sets the pH, release of the rare earths from the solid, and their loss from solution. For each process we used a rate law or equilibrium from the literature where one was available. Where we could not find a form suited to the whole data set, we used the simplest form consistent with the behaviour of the compiled runs and state the assumptions behind it. The same three-host description of the solid is used in LixaLearn (Asgari, 2026b).

Acid production. We are not aware of a rate law that describes acid production across all five organism groups, and most studies report acid at only a few times. We therefore describe it with an empirical curve that has a lag, a maximum rate and a plateau. These are the three features used to describe microbial growth curves (Zwietering et al., 1990), and Pedram et al. (2020) fitted curves of this kind to the growth of Aspergillus niger on red mud. The simplest such curve is a first-order approach to a maximum after a lag,

$$C_{bio}(t) = A\left[1 - e^{-k\,(t\,-\,t_{lag})}\right]_{+}, \tag{1}$$

where C_{bio} is the acid made (mM, proton equivalents), A the largest amount, k the production rate (d^{-1}), t_{lag} the lag (d) and $[x]_{+} = \max(x, 0)$. Three assumptions are made. First, acid production does not depend on the residue, so inhibition by alkalinity or by released metal is ignored. Second, each organism group makes one effective acid. This is citric acid for fungi, gluconic acid for acetic acid bacteria and other heterotrophs, and sulfuric acid for acidophiles, the main acids these groups excrete (Gadd, 2010; Barmettler et al., 2016). Fungi also make a fitted fraction f_{ox} of oxalic acid (Gadd, 2010). Third, acid is counted in proton equivalents. In two-step runs the organism has grown for t_{pre} days before the residue is added, so the lag becomes $-t_{pre}$. Spent-medium runs start with $C_{bio} = A$ and make no more acid. Chemical-acid runs use the acid and concentration stated by the authors. The starting acidity of the medium is converted to a fully dissociated strong-acid equivalent, $C_{med} = 10^{3} \times 10^{-pH_0}$ mM.

Release of base by the residue. Alkaline residues release base as their soluble and slowly soluble alkaline phases dissolve. In red mud these include sodium hydroxide, carbonates, aluminates and sodalite-type phases (Gräfe et al., 2011). We describe this release by first-order kinetics towards a base capacity proportional to the solids loading. We further assume that the acid-soluble host consumes acid in proportion to the fraction of it that has dissolved, so that dissolution of the host and release of its rare earths are congruent. The base in solution is then

$$B(t) = c\,\rho\left[1 - e^{-k_B\,(t\,-\,t_{add})}\right]_{+} + c_{mat}\,\rho\,X_1(t), \tag{2}$$

where ρ is the solids loading (g L^{-1}), t_{add} the time the residue was added, c the base capacity of the residue (mmol g^{-1}), k_B its release rate (d^{-1}), c_{mat} the acid consumed per gram of dissolved acid-soluble host (mmol

g^{-1}) and X_l the dissolved fraction of that host (Eq. 7). Both c and k_B are properties of the residue. The released base is treated as a single buffer with the first dissociation constant of carbonic acid, pK = 6.4 at 25 °C (Stumm and Morgan, 1996).

Charge balance and pH. The free proton concentration h (mol L^{-1}) follows from electroneutrality of the solution (Stumm and Morgan, 1996),

$$h + B\,\frac{h}{h + K_{a,B}} = \sum_i C_i\, n_i\, \frac{K_{a,i}}{K_{a,i} + h} + \frac{K_w}{h}, \tag{3}$$

where the sum runs over the chemical acid, the biogenic acid and the medium acidity, C_i are their concentrations (mol L^{-1}), n_i the protons counted per molecule, $K_{a,i}$ their dissociation constants, $K_{a,B}$ = $10^{-6.4}$ and K_w = 10^{-14}. The equation assumes that activities equal concentrations, which ignores ionic-strength corrections. It also treats each organic acid as monoprotic, using only its first dissociation constant, and ignores the charge of medium salts and released metals. The pK values at 25 °C (Extended Data Table 1) are from the CRC Handbook (Haynes, 2016), except gluconic acid (Sawyer, 1964). Sulfuric and hydrochloric acid are taken as fully dissociated, and sulfuric acid gives two protons. The organic acid mixtures of one study are given an effective pK of 3.7 (our assumption). Eq. (3) is solved at every time step in double precision, by bisection in log h started from the previous step and then two Newton steps that carry the gradient.

The free complexing ligand and free oxalate are the deprotonated fractions of the complexing acids, from the same monoprotic speciation (Stumm and Morgan, 1996),

$$L = \sum_i C_i\, \ell_i\, \frac{K_{a,i}}{K_{a,i} + h}, \qquad L_{ox} = \sum_i C_i\, o_i\, \frac{K_{a,i}}{K_{a,i} + h}, \tag{4}$$

where ℓ_i is one for a complexing acid (citric, gluconic, oxalic, lactic, succinic) and zero otherwise, and o_i is one for oxalic acid and f_{ox} for the biogenic acid of fungi. The ligand is assumed to be in excess of the released metal, so complexation does not lower L.

Temperature. All rate constants depend on temperature through an Arrhenius factor relative to 25 °C (Levenspiel, 1999),

$$\alpha(T) = \exp\left[-\frac{E_a}{R}\left(\frac{1}{T} - \frac{1}{298.15\ \mathrm{K}}\right)\right], \tag{5}$$

where E_a is an apparent activation energy and R the gas constant. A single E_a is assumed for all residues, because only one development study varied temperature. The diffusion-limited host uses $\sqrt{\alpha}$, which corresponds to half the activation energy. This reflects the weaker temperature dependence of diffusion and is our assumption.

Release from the solid. The rare earths sit in four hosts with shares s_0 to s_3 that sum to one, as in LixaLearn (Asgari, 2026b). Rare earths held on clay and oxide surfaces are released by ion exchange (Moldoveanu and Papangelakis, 2012). We describe the exchanged fraction by a Langmuir isotherm,

$$X_0 = \frac{K_{ex}\, a}{1 + K_{ex}\, a}, \qquad a = h + \kappa_x L, \tag{6}$$

where K_{ex} is the exchange constant (L mol^{-1}) and a the concentration of displacing species, protons plus ligand weighted by κ_x. Two assumptions are made. Exchange is at equilibrium at all times, because it is

fast compared with the sampling interval of the compiled runs (hours to days). Protons and ligand compete for the same sites.

The acid-soluble host dissolves by the shrinking-core model under surface-reaction control (Levenspiel, 1999). Its rate constant adds a proton-promoted and a ligand-promoted term, as found for the dissolution of oxides by Furrer and Stumm (1986),

$$\frac{dX_1}{dt} = 3\,k_r\,(1-X_1)^{2/3}, \qquad k_r = k_{r0}\,(h^{\,n} + \kappa L)\,\alpha(T), \tag{7}$$

where k_{r0} is a rate constant (d^{-1} for h in mol L^{-1}), n the reaction order in protons, kept between 0.3 and 1.5, and κ the strength of ligand-promoted dissolution. The shrinking-core form assumes grains of one size that dissolve from the outside in.

The diffusion-limited host follows the shrinking-core model under control by diffusion through a product layer (Levenspiel, 1999). Its driving force is taken to be proportional to h + κL (our assumption),

$$1 - 3(1-X_2)^{2/3} + 2(1-X_2) = \int_0^{\,t} k_{d0}\,(h+\kappa L)\,\sqrt{\alpha(T)}\,;dt\,', \tag{8}$$

where k_{d0} is a rate constant (L mol^{-1} d^{-1}). The fourth, locked host releases nothing.

Losses from solution. Rare earth oxalates are poorly soluble, and oxalic acid is used to precipitate rare earths from leach solutions (Zhang et al., 2021). Rare earth ions also hydrolyse and precipitate as the pH rises (Baes and Mesmer, 1976). As we could not find rate laws for these losses that apply across the compiled runs, both are described with empirical saturating functions. Recovery is

$$R(t) = (s_0X_0 + s_1X_1 + s_2X_2)\Big(1 - \theta\tfrac{L_{ox}}{L_{ox}+K_{ox}}\Big)\Big(1 - \tfrac{1}{1+e^{-(\mathrm{pH}-\mathrm{pH}_p)/0.25}}\Big), \tag{9}$$

where θ is the largest fraction lost to oxalate, K_{ox} the free oxalate at half that loss and pH_p the pH at which half the metal is lost to hydrolysis. Three assumptions are made. The two losses act independently and on all hosts alike. The loss responds at once to the solution. The hydrolysis step has a fixed width of 0.25 pH units. Time is integrated explicitly on 80 equal steps from zero to the last observation of each run, so that the acid used up by dissolution at one step changes the pH at the next.

2.3 Parameter sharing and fitting

The parameters are shared across studies by partial pooling, as in hierarchical models (Gelman et al., 2013), at four levels (Extended Data Table 2). The global parameters are κ, κ_x, θ, K_{ox}, pH_p and E_a. Each organism group has A, k, t_{lag}, t_{pre} and f_{ox}. Each residue and element class (scandium or the other rare earths) has the host shares, k_{r0}, n, k_{d0}, K_{ex}, c, k_B and c_{mat}. Each run has shifts of log A, t_{lag}, log k_{r0} and log c, and each series has shifts of the host shares. Every parameter has a weak normal prior on an unconstrained scale (Extended Data Table 2). The run and series shifts have standard normal priors, so they stay small unless the data require otherwise. All parameters were fitted together by minimising

$$\mathcal{L} = \sum_s w_s\left[\sum_j\Big(\frac{\hat{R}_{sj}-R_{sj}}{\sigma_R+u_{sj}}\Big)^2 + \sum_j\Big(\frac{\widehat{\mathrm{pH}}_{sj}-\mathrm{pH}_{sj}}{\sigma_{pH}}\Big)^2 + \sum_j\Big(\frac{\hat{C}_{sj}-C_{sj}}{5+0.2\,C_{sj}}\Big)^2\right] + \mathcal{P}, \tag{10}$$

where s runs over series and j over measurements, hats mark model values, u_{sj} is the extraction uncertainty and $\mathcal{P}$ the prior penalty. This is a weighted least-squares loss, which corresponds to

independent normal errors. The error scales are our choices. They are σ_R = 0.03 (as a fraction) for recovery, σ_{pH} = 0.25 for pH, and 5 mM plus 20 % for acid C (mM), which allows for the uncertain relation between measured and free acid. For acidophiles, whose acid is reported as sulfate, increments from the first measurement are compared. The weight $w_s = 1/\sqrt{N}$, with N the number of measurements in the study of series s, keeps the largest studies from dominating the fit. The loss was minimised with Adam (Kingma and Ba, 2015) for 1500 steps at a learning rate of 0.02, with a cosine schedule and gradient clipping, in PyTorch (Paszke et al., 2019). Because the loss equals minus twice the log posterior up to a constant, approximate uncertainties of the organism-group parameters were taken from the inverse of its curvature at the optimum (MacKay, 1992), with all other parameters fixed.

2.4 Kinetic models fitted run by run

For comparison, four kinetic models were fitted by least squares (SciPy) to each development run with at least four recovery points. Each uses the contact time $\tau = \max(t - t_{add}, 0)$. First-order kinetics gives $R = R_{max}(1 - e^{-k\tau})$. The shrinking-core model gives $1 - (1 - X)^{1/3} = k\tau$ under reaction control and $1 - 3(1 - X)^{2/3} + 2(1 - X) = k\tau$ under diffusion control, both with $R = R_{max} X$ (Levenspiel, 1999). The Avrami model gives $R = R_{max}[1 - e^{-(k\tau)^m}]$ (Avrami, 1939). Each fit was started from three rate values, and the best fit was kept.

2.5 Prediction from the first points of a run

To predict a new run, BioLixa keeps all global, group and residue parameters of the fitted model fixed and updates only the parameters of that run from its first k recovery points. This is a form of data assimilation: the early observations of the run update its run shifts and the share shifts of its series, and the priors of those shifts act as the background state. Residue and element classes not seen in development take the mean of the development values. With few points the update has several minima, because release starts only after the acid has overcome the alkalinity of the residue. It is therefore started from 27 combinations of acid amount, lag and rate shifts and run for 200 Adam steps at a learning rate of 0.05. The resulting forecasts are averaged with weights $\exp(-\Delta L/2)$, where ΔL is the loss of a start above the lowest.

We compared two assimilation schemes. The first scheme assimilates the first k recovery points only. Its details were chosen among six variants in the development rehearsal, by a rule written before the comparison: the lowest mean error at k = 2 over the five rehearsal studies, with variants within 0.1 points treated as tied and ties broken at k = 3. The chosen variant frees the shifts of log A and t_{lag} only, with prior standard deviation 0.5. After the held-out test, an analysis of the errors showed that the first scheme ignored the pH measurements made before the k-th recovery point, although these carry the information on acid supply that the model lacks. The second scheme therefore also assimilates those pH measurements, with the same error scale as in the fit (σ_{pH} = 0.25). It was chosen among four variants (with and without early pH, with and without a correction that shifts the forecast through the last known point) by the same kind of rule, again written before the comparison and applied to the development rehearsal only. Both schemes use only information that a laboratory would have at the time of the k-th recovery point.

The data-driven baselines received the same information. Their inputs were one-hot codes of organism group, mode and residue, a scandium flag, temperature and starting pH. They also received the logarithms (plus one) of solids loading, chemical acid concentration, time and contact time. They were trained on all development runs plus the k known points of the new runs. The known points were weighted ten times, or repeated ten times for methods without sample weights. The regressors were

histogram gradient boosting (300 iterations, learning rate 0.05), a random forest (300 trees, minimum leaf size 2), support vector regression (RBF kernel, $C = 10$, $\varepsilon = 1$, standardised inputs), three nearest neighbours and a neural network with two hidden layers of 64 units, all from scikit-learn (Pedregosa et al., 2011). The simple rules were the last known value and a straight line in $\log(1 + t)$ through the known points (for $k \geq 2$). The error of a run is the mean absolute error over its points after the first k. The error of a study is the mean over its runs.

2.6 Held-out protocol

The held-out studies were chosen on 29 October 2026 from the study summaries, before any model was run. One study was taken for each organism group with recovery time series, on four different residues. The protocol fixed the task, the baselines and the success criterion. The task used runs with at least four recovery points, of which the first $k = 1$, 2 or 3 were known. Success required a lower mean error than every baseline at $k = 2$, over the four studies, and a lower error than every baseline in at least three of the four studies. The rule for choosing among the variants of the first scheme was written on 30 October 2026, before they were compared. The code was then frozen with a version-control tag and checksums, and the held-out test of the first scheme was run once. The second scheme was developed afterwards on the development studies only, frozen with its own tag, and then run once on the same held-out studies. Because these studies had already been used to evaluate the first scheme, the second evaluation is not blind, and we report it as a comparison of the two schemes, not as a second independent test.

3 Results

3.1 A compiled record of microbial rare earth leaching

Nineteen papers on rare earth bioleaching from residues were collected, and the data of 18 were extracted (Methods). One paper reported no rare earths and was rejected. One study of chemical Fenton leaching was excluded because no organism was involved. The remaining 17 studies (Table 1, Fig. 2) contain 217 runs on 10 residues. These are red mud and bauxite residue, coal fly ash, coal waste, phosphogypsum, spent car and cracking catalysts, circuit boards, e-waste dust, lamp phosphor and LED lamps. The organisms are fungi, acetic acid bacteria, sulfur-oxidising acidophiles, yeasts and other heterotrophs. The runs give 821 recovery measurements in 362 series (one series per run and element), 1082 pH measurements and 531 acid measurements.

Before any model was built, four studies were set aside for a single final test. We chose one study for each organism group with recovery time series, each on a different residue. They are Kiskira et al. (2023), with Aspergillus niger on bauxite residue, Zhang et al. (2025), with Gluconobacter oxydans on phosphogypsum, Shi et al. (2026), with Acidithiobacillus ferrooxidans on coal fly ash, and Marra et al. (2018), with Acidithiobacillus thiooxidans on e-waste dust. Together they hold 50 runs and 269 recovery points. The other 13 studies were used to build and fit the model. They hold 552 recovery, 819 pH and 531 acid measurements.

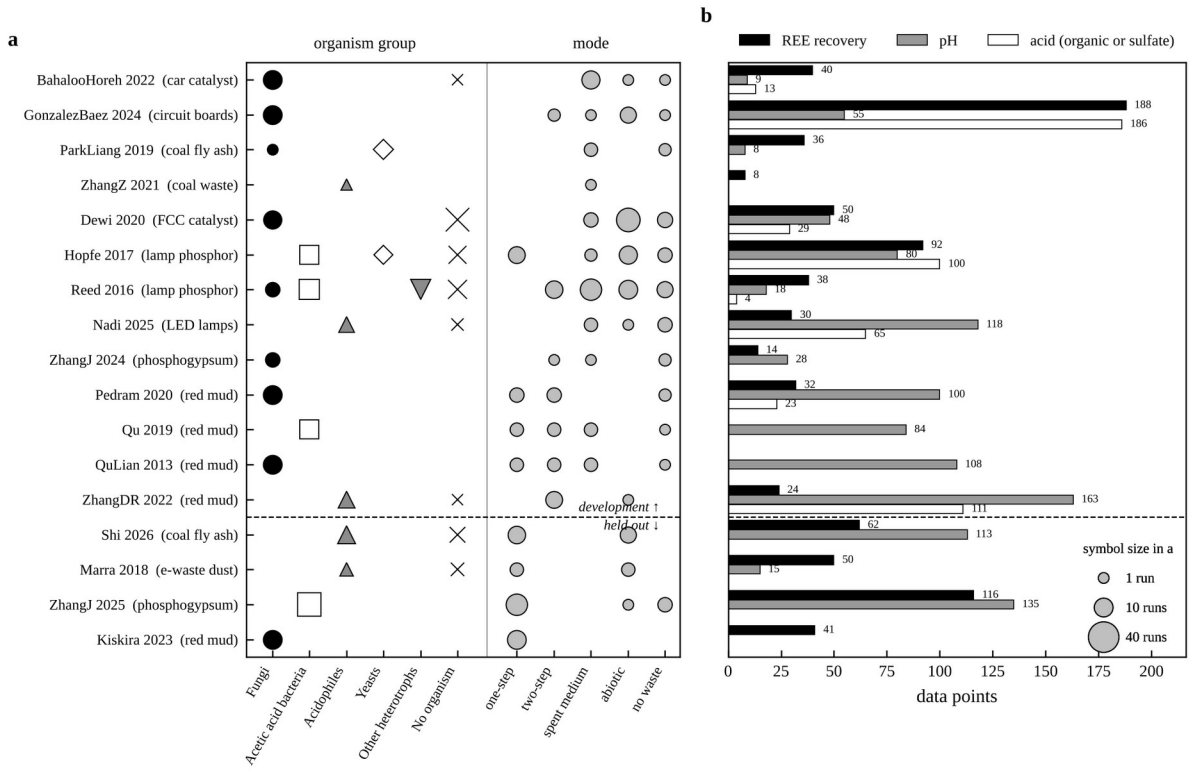


Figure 2. The compiled data. (a) Organism groups and leaching modes in each study; symbol area grows with the number of runs. (b) Number of recovery, pH and acid measurements in each study. Studies below the dashed line were held out for the final test.

Table 1. The compiled studies. Studies marked * were held out for the final test. Modes: one-step, two-step, spent medium and abiotic (chemical acid or sterile control). Solids, solids loading (w/v); T, temperature; Days, longest time sampled; n.r., not reported.

Study	Residue	Organism groups	Modes	Solids (%)	T	Days	Runs	Best recovery, % (element)
Bahaloo-Horeh and Mousavi (2022)	car catalyst	Fungi	spent medium, abiotic	1–3	30–60 °C	14	11	51.3 (Nd)
Dewi et al. (2020)	FCC catalyst	Fungi	spent medium, abiotic	5	30 °C	14	29	85.1 (La)
Gonzalez Baez et al. (2024)	circuit boards	Fungi	two-step, spent medium, abiotic	1	25 °C	7	10	85.0 (Gd)
Hopfe et al. (2017)	lamp phosphor	Acetic acid bact., Yeasts	one-step, spent medium, abiotic	2.74–2.83	n.r.	14	22	67.9 (Y)
Kiskira et al. (2023) *	red mud	Fungi	one-step	1–10	30 °C	20	10	46.4 (Sc)
Marra et al. (2018) *	e-waste dust	Acidophiles	one-step, abiotic	0.5–2	30 °C	8	6	100.0 (Ce)
Nadi et al. (2025)	LED lamps	Acidophiles	spent medium, abiotic	1–5	30 °C	29	8	80.0 (Nd)
Park and Liang (2019)	coal fly ash	Fungi, Yeasts	spent medium	1	28 °C	9	5	67.7 (Yb)
Pedram et al. (2020)	red mud	Fungi	one-step, two-step	3	30 °C	20	10	38.1 (Sc)
Qu et al. (2019)	red mud	Acetic acid bact.	one-step, two-step, spent medium	2–10	30 °C	30	10	pH only
Qu and Lian (2013)	red mud	Fungi	one-step, two-step, spent medium	2–10	30 °C	50	10	pH only

Study	Residue	Organism groups	Modes	Solids (%)	T	Days	Runs	Best recovery, % (element)
Reed et al. (2016)	lamp phosphor	Acetic acid bact., Fungi, Other heterotr.	two-step, spent medium, abiotic	1.5	30 °C	9	39	49.2 (total)
Shi et al. (2026) *	coal fly ash	Acidophiles	one-step, abiotic	2–10	30 °C	14	14	40.4 (total)
Zhang et al. (2022)	red mud	Acidophiles	two-step, abiotic	0.5–0.6	45 °C	27	8	91.4 (Y)
Zhang et al. (2024)	phosphogypsum	Fungi	two-step, spent medium	n.r.	30 °C	15	4	44.2 (total)
Zhang et al. (2025) *	phosphogypsum	Acetic acid bact.	one-step, abiotic	6.25–50	20–44 °C	30	20	23.3 (Nd)
Zhang et al. (2021)	coal waste	Acidophiles	spent medium	42.9	35 °C	3	1	4.9 (total)

3.2 One parameter set across thirteen studies

BioLixa was fitted to all development studies at once. Each organism group has one acid amount, production rate and lag. Each residue and element class has one set of host shares, rates and alkalinity. Each run may shift its acid amount, lag, rate and alkalinity, but these shifts are pulled towards zero. With this structure the model reproduced 552 recovery measurements with a mean absolute error of 2.3 percentage points and $R^2 = 0.97$ (Fig. 4, Table 2). It reproduced 811 pH measurements with a mean absolute error of 0.54 pH units and $R^2 = 0.85$. The recovery error was smallest for Hopfe et al. (2017) (0.7 points) and largest for Zhang et al. (2022) (5.1 points).

Fig. 3 shows one run for each organism group. In the two-step fungal run on circuit boards (Fig. 3a), the pH of the culture falls as acid is made and rises again when the residue is added on day 3. Recovery jumps within hours of the addition. In the chemical-acid run on the same residue (Fig. 3e), the pH only rises, because no new acid is made and the residue slowly neutralises the acid that was added. The model follows both runs. It also follows the fall of recovery after day 4 in the chemical-acid run, which it explains by hydrolysis as the pH rises. The spent-medium runs (Fig. 3b, d) are fitted less closely. Their recovery scatters from one sample to the next, and the model passes a smooth curve through the scatter. Supplementary Figs S1 to S13 show every fitted run, and Extended Data Fig. 1 shows the residuals of each study.

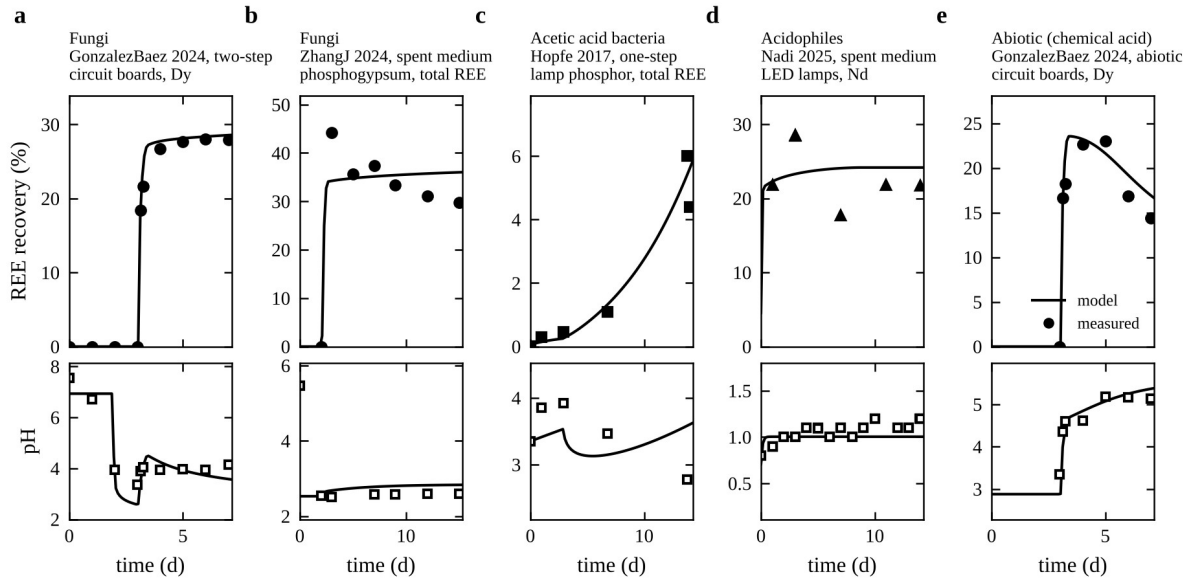


Figure 3. Fits for each organism group. Top row, rare earth recovery; bottom row, pH, on the same time axis. Lines are the fitted model and symbols the measurements. (a) Penicillium expansum, two-step, circuit boards, dysprosium (Gonzalez Baez et al., 2024). (b) Aspergillus niger spent medium, phosphogypsum, total rare earths (Zhang et al., 2024). (c) Kombucha consortium, one-step, lamp phosphor, total rare earths (Hopfe et al., 2017). (d) Acidithiobacillus thiooxidans spent medium, LED lamps, neodymium (Nadi et al., 2025). (e) Chemical organic acid mix (mainly gluconic acid) added with the residue on day 3, circuit boards, dysprosium (Gonzalez Baez et al., 2024).

The organic acid is fitted poorly. Over 76 measured acid concentrations the mean absolute error was 52 mM, and the median ratio of model to measured acid was 0.05 (Fig. 4c). The highest measured values, 125 to 190 mM of citric, gluconic, acetic or oxalic acid, come from fungal fermentations and Kombucha cultures whose pH stayed between about 2 and 4. If all of this acid released its protons, the pH would be lower than measured. The fit gives more weight to pH and recovery, which have more data. Part of the measured acid is therefore probably not free acid. It may be buffered by the medium or partly neutralised by the base used to set the starting pH. It may also have been measured as total carboxylate. The model has no term for any of these effects, and this sets one of its limits (Discussion).

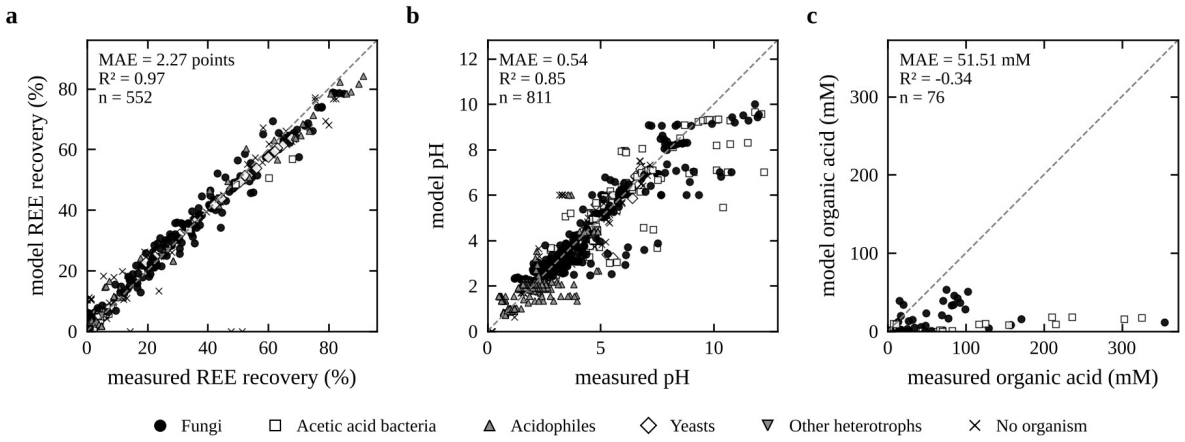


Figure 4. Model against measurement for all development data. (a) Rare earth recovery, (b) pH, (c) organic acid. Symbols mark the organism group; the dashed line is 1:1. Each panel gives the mean absolute error (MAE), R^2 and the number of measurements n. Sulfate data of acidophiles, which are fitted as increments, are not shown in (c).

Table 2. Fit statistics of the development fit for each study. MAE, mean absolute error. R^2 is low for studies whose recoveries span a narrow range (for example the single coal waste run).

Study	Recovery n	Recovery MAE (points)	Recovery R^2	pH n	pH MAE	pH R^2
Bahaloo-Horeh and Mousavi (2022)	40	4.65	0.10	9	0.27	0.92
Dewi et al. (2020)	50	4.33	0.96	42	0.16	0.98
Gonzalez Baez et al. (2024)	188	1.90	0.99	55	0.31	0.94
Hopfe et al. (2017)	92	0.70	0.95	80	0.38	0.86
Nadi et al. (2025)	30	3.01	0.95	118	0.54	-0.04
Park and Liang (2019)	36	1.61	0.98	8	0.17	0.95
Pedram et al. (2020)	32	1.82	0.95	100	0.39	0.85
Qu et al. (2019)	0	–	–	84	0.99	0.53
Qu and Lian (2013)	0	–	–	108	0.81	0.78
Reed et al. (2016)	38	1.20	0.99	16	0.29	0.95
Zhang et al. (2022)	24	5.06	0.96	163	0.53	0.76
Zhang et al. (2024)	14	2.79	0.90	28	0.60	0.22
Zhang et al. (2021)	8	1.72	-1.37	0	–	–
All development studies	552	2.27	0.97	811	0.54	0.85

3.3 What the fitted model says about bioleaching

The fitted acid production differs between organism groups (Fig. 5a, Extended Data Fig. 6). Acidophiles reached 39 mM proton equivalents at a rate of 0.32 per day after a lag of 0.9 days. Fungi reached 29 mM at 0.07 per day after 2.2 days, and acetic acid bacteria reached 18 mM. These are effective amounts. They are the acid that the pH and recovery data require, and they are well below the measured organic acid for the reasons given above.

The residue has a strong effect on its own leaching. Fig. 5b and c follow a one-step fungal run on red mud at three solids loadings, using the fitted parameters. At 1 % solids the fungus lowers the pH from 9.0 to 3.1 within three weeks and releases 66 % of the rare earths. At 5 % the alkalinity of the residue keeps the pH at 6.5, and recovery stays below 2 %. At 15 % almost nothing is released. The organism makes the same

acid in all three runs, and the extra residue neutralises it. The fit follows the measured fall of recovery with solids loading for LED lamps (Nadi et al., 2025; Extended Data Fig. 2b). For spent car catalyst (Bahaloo-Horeh and Mousavi, 2022; Extended Data Fig. 2a, c), the measured recovery of lanthanum and neodymium rose with solids loading between 1 and 2.5 %. The fit follows that rise, but it overestimates cerium and praseodymium and the recovery at 30 to 50 °C. The fitted alkalinity was highest for LED lamp powder and red mud (Table 3), the two residues where solids loading had the largest effect.

The host shares show where the releasable metal sits (Fig. 5d, Table 3). In red mud the model places 51 % of the rare earths on exchange sites and 38 % in a slowly leached host. Most of the scandium, 55 %, is in the slow host. In circuit boards 46 % is in an acid-soluble host. For spent car catalyst and lamp phosphor, 84 and 79 % of the metal is in no host that the acids of the development runs could reach. These shares come from leaching curves alone. They describe what the leaching data require and are not a measured mineralogy.

The solution chemistry gives two more results. At the same dose of 50 mM on red mud, the model gives 80 % recovery after 7 days for citric acid, 78 % for gluconic, 82 % for sulfuric and 69 % for oxalic acid (Fig. 5f). Oxalic acid gives the lowest pH of the organic acids but also the lowest recovery, because part of the released metal precipitates as oxalate. The fitted largest oxalate loss is 23 %. With chemical citric acid, each residue has a threshold dose set by its alkalinity, and below it almost nothing is released. At 5 % solids the threshold is about 20 mM for cracking catalyst, 50 mM for red mud and 100 mM for circuit boards (Fig. 5e). Above the threshold, recovery levels off at the share of the metal that the acid can reach. Extended Data Figs 4 and 5 give the full response surfaces and titration curves. Extended Data Fig. 3 compares measured and fitted recovery across leaching modes.

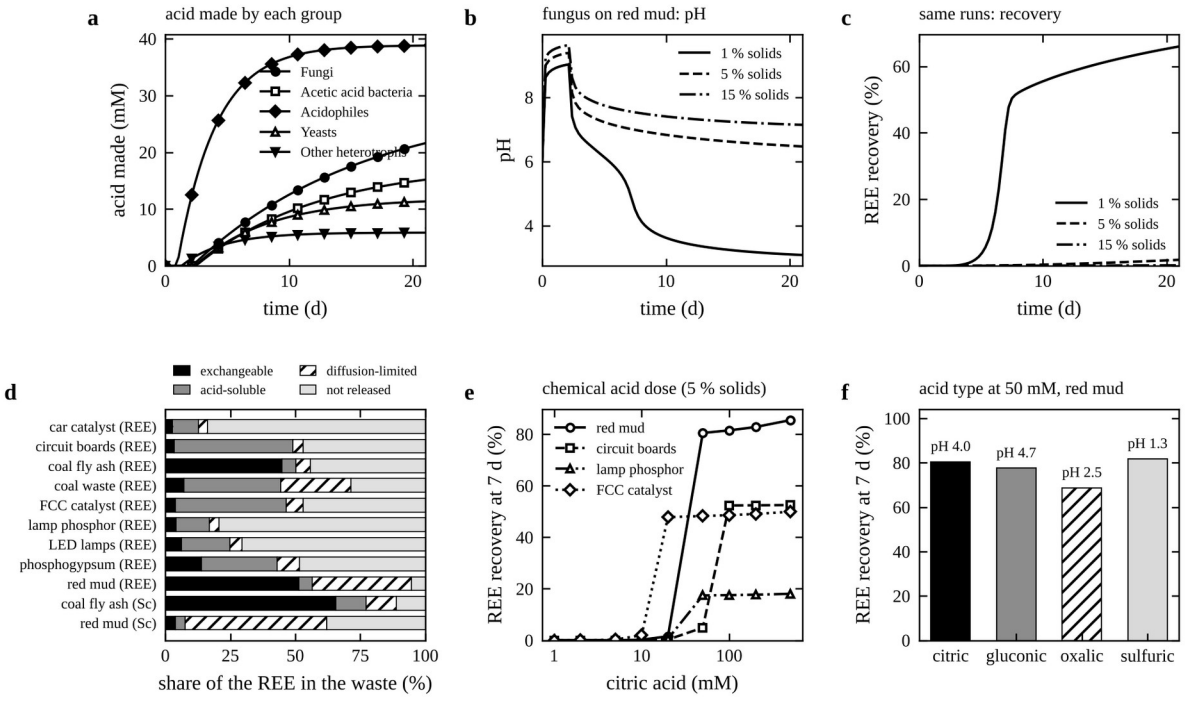


Figure 5. What the fitted model says. (a) Acid made by each organism group in culture without residue. (b, c) pH and recovery for Aspergillus niger in one-step contact with red mud at 1, 5 and 15 % solids. (d) Fitted shares of the rare earths (and scandium) in each host. (e) Recovery after 7 days against the dose of chemical citric acid at 5 %

solids. (f) Recovery and final pH after 7 days for four acids at 50 mM on red mud. All panels are model output with the development parameters.

Table 3. Fitted host shares, alkalinity and acid use of each residue (development fit). REE, total or individual rare earths other than scandium.

Residue	Element	Exchangeable (%)	Acid-soluble (%)	Diffusion-limited (%)	Not released (%)	Alkalinity (mmol g^{-1})	Acid use (mmol g^{-1})
Car catalyst	REE	3	10	3	84	0.45	1.02
Circuit boards	REE	3	46	4	47	0.35	1.19
Coal fly ash	REE	45	6	5	44	0.33	0.81
Coal fly ash	Sc	66	12	12	11	0.65	0.52
Coal waste	REE	7	37	27	29	0.17	0.68
Cracking catalyst	REE	4	43	6	47	0.30	0.06
Lamp phosphor	REE	4	13	4	79	0.01	0.77
LED lamps	REE	6	18	5	70	1.61	1.37
Phosphogypsum	REE	14	29	9	48	0.07	0.03
Red mud	REE	51	5	38	5	0.85	0.09
Red mud	Sc	4	4	55	38	0.85	0.09

3.4 Comparison with kinetic models fitted run by run

Bioleaching curves are usually analysed by fitting a kinetic model to each curve alone. We fitted four such models to each of the 52 development runs with at least four recovery points (Methods). They were first-order kinetics, the shrinking core with reaction control, the shrinking core with diffusion control, and the Avrami model. On the same 319 points, these fits gave mean absolute errors from 0.95 (Avrami) to 1.32 points. BioLixa gave 1.47 (Table 4, Extended Data Fig. 7). The per-run models fit single curves slightly better, which is expected because each run has its own two or three parameters. BioLixa uses 157 shared parameters for all studies, plus run shifts that are pulled towards zero, and it fits pH and acid at the same time. Its root-mean-square error (2.55) is the lowest of the five, because it avoids the few large misses of the per-run fits on short or noisy runs. The per-run models cannot predict a run at another solids loading or with another organism. BioLixa can, and the next two sections test how well.

Table 4. BioLixa and four kinetic models fitted run by run, on the 319 recovery points of development runs with at least four points.

Model	Fitted to	Parameters	MAE (points)	RMSE (points)	Predicts new conditions
First order	each run	104	1.23	2.78	no
Shrinking core, reaction	each run	104	1.32	2.92	no
Shrinking core, diffusion	each run	104	1.22	2.78	no
Avrami	each run	156	0.95	2.63	no
BioLixa	all studies at once	157 shared + 1748 run shifts	1.47	2.55	yes

3.5 Predicting the rest of a run from its first points

The test of prediction follows a common laboratory situation. The first one, two or three recovery points of a new run are known, and the rest must be predicted. BioLixa refits only the shifts of that run to the known points and keeps all other parameters (Methods). It was compared with five data-driven regressors trained on the same inputs. These were gradient boosting, a random forest, support vector regression, nearest neighbours and a neural network. Two simple rules were also used. One holds the last known value constant, and the other fits a straight line in the logarithm of time.

The method was first rehearsed on the development data. Each of five development studies was left out in turn, the model was refitted without it, and its 51 runs were predicted (Fig. 6). Six variants of the first assimilation scheme were compared in this rehearsal, using a selection rule written before the comparison (Methods). The two best variants were within 0.1 points at two known points (12.69 and 12.75), and the rule broke the tie at three known points. No variant came close to holding the last value, which gave 7.7 points. With the chosen variant of the first scheme, BioLixa had a mean error of 12.5 points with one known point, 12.8 with two and 16.0 with three. The best baseline reached 12.7 (gradient boosting), 7.7 (the last value) and 6.1 (the last value). With one known point BioLixa had the lowest mean error, but only by 0.2 points, and it was the best method in two of the five studies. In 49 of the 52 development runs with at least four points, the first point is at the start of contact or below 0.5 % recovery. With one known point, the task is then close to predicting a run from its conditions alone. With two or more known points, holding the last value was the most accurate method. At two known points BioLixa beat it in only 12 of 51 runs (Extended Data Fig. 8).

The errors differ strongly between studies (Fig. 6b). At two known points, BioLixa and the last value gave circuit boards 15.6 against 14.5, lamp phosphor 1.1 against 1.0, LED lamps 3.5 against 2.5, red mud 24.0 against 14.6, phosphogypsum 19.5 against 6.0 points. The largest errors come from runs in which recovery is still rising when the known points end. The model must then estimate how much acid the organism will

still make, and two recovery points say little about it. In the red mud runs of Pedram et al. (2020), the model expected too little further acid and predicted almost no further release, while the measured recovery kept rising (Fig. 6f). The last value was closer.

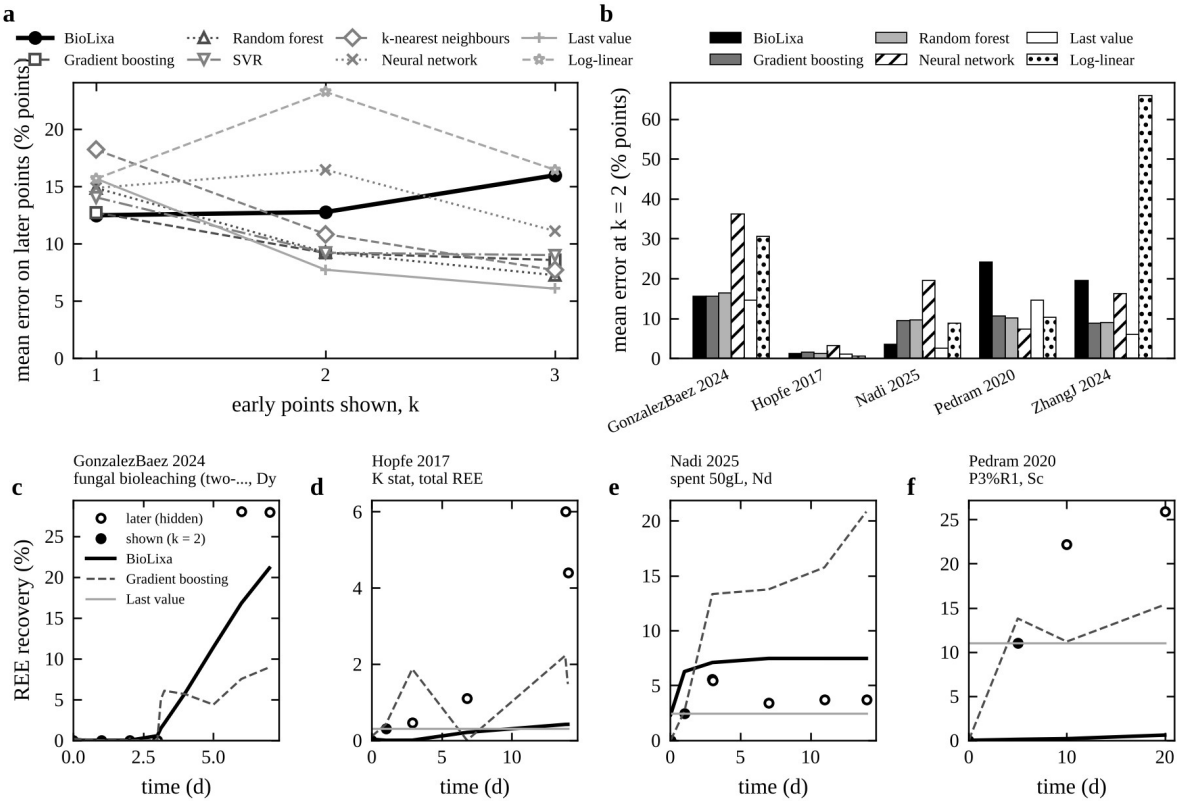


Figure 6. Development rehearsal: each of five development studies was left out in turn, the model refitted without it, and its runs predicted from their first k recovery points. (a) Mean error on the remaining points over the five studies against k. (b) Error at k = 2 for each study and method. (c to f) Examples at k = 2: filled circles are the two known points, open circles the later points the methods did not see.

3.6 Assimilating early pH measurements

The errors of the first scheme had a clear pattern. They were largest in runs where recovery was still rising after the known points, because the model then has to guess how much acid the organism will still make. The early pH measurements contain this information: a pH that stays high means little free acid, and a falling pH means acid is accumulating. In the five rehearsal studies, a mean of 2 to 4.5 pH measurements per run were available before the second recovery point. The second assimilation scheme uses them (Methods).

With early pH assimilated, the mean rehearsal error at two known points fell from 12.8 to 8.9 points, a reduction of 30 %, and at three known points from 16.0 to 7.9 points, a reduction of 50 % (Fig. 7a, Table 5). At two known points BioLixa then had a lower error than all five data-driven regressors, including gradient boosting (9.2 points). At three known points it was close to the best of them (random forest, 7.2 points). Only the last known value remained clearly more accurate (7.7 and 6.1 points). The largest gain was on red mud (Pedram et al. (2020)), where the error at two known points fell from 24.0 to 9.0 points,

below the last value (14.6). There the early fall of pH told the model that acid was accumulating, and it predicted the continued rise of recovery that the first scheme had missed (Fig. 7c). With only one known point, the first scheme remained better (12.5 against 15.1 points), because the pH measured at the very start of a run constrains the acid supply poorly. The correction through the last known point helped less than the pH (Table 5).

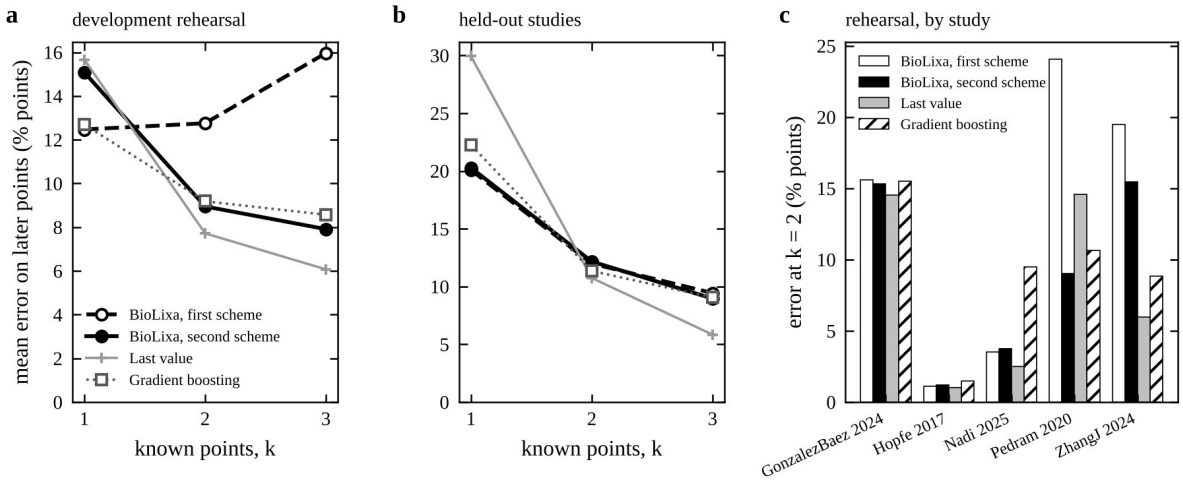


Figure 7. The two assimilation schemes compared. The first scheme assimilates the first k recovery points of a new run; the second also assimilates the pH measured up to the k-th recovery point. (a) Development rehearsal and (b) held-out studies: mean error on the later points against k, with the last known value and gradient boosting for comparison. (c) Rehearsal error at k = 2 for each study.

3.7 Held-out test

The protocol of the final test was written before any model was built (Methods). The test was run once, after the code had been frozen. It used the four held-out studies, with 35 runs that have at least four recovery points, and the same task and baselines as the rehearsal. Success required two things at two known points. BioLixa had to have a lower mean error than every baseline, and a lower error than every baseline in at least three of the four studies.

With the first assimilation scheme, BioLixa had a mean error of 20.1 points with one known point, 12.0 with two and 9.4 with three (Fig. 8). The best baseline reached 22.2 (gradient boosting), 7.8 (a neural network) and 5.8 (the last value). At two known points, which the protocol used, BioLixa had the highest mean error of the eight methods and was not the best method in any study. The success criterion was therefore not met. The rehearsal pattern was repeated. BioLixa was the most accurate method with one known point and fell behind when more points were known.

The advantage at one known point was uneven. Most of it came from the e-waste dust of Marra et al. (2018). There, recovery rose from near zero to near complete within the run, and every method missed by tens of points (BioLixa 54, gradient boosting 63, last value 88). BioLixa was the best method with one known point in one of the four held-out studies. At two known points it reached 16.4 points on bauxite residue (best baseline 9.2), 15.2 points on e-waste dust (best baseline 6.5), 5.9 points on coal fly ash (best baseline 3.1), 10.6 points on phosphogypsum (best baseline 3.9). The bauxite residue of Kiskira et al. (2023)

is the only held-out residue of a type used in development. The error there was no smaller than on the residues the model had not seen.

The second scheme, which also assimilates early pH, was then run once on the same four studies (Fig. 7b, Table 5). Its mean errors were 20.3, 12.2 and 9.0 points with one, two and three known points, close to those of the first scheme (20.1, 12.0 and 9.4). The gain seen in the rehearsal did not carry over. The held-out studies had fewer early pH measurements than the rehearsal studies: none before the second recovery point in Kiskira et al. (2023), 1.3 per run in Zhang et al. (2025) and 2 in Marra et al. (2018). Where pH was most frequent, on the coal fly ash of Shi et al. (2026) (4 per run), all runs had reached at least half their final recovery by the second point, so there was little left for the pH to explain. Both schemes kept the lowest error of all eight methods with one known point.

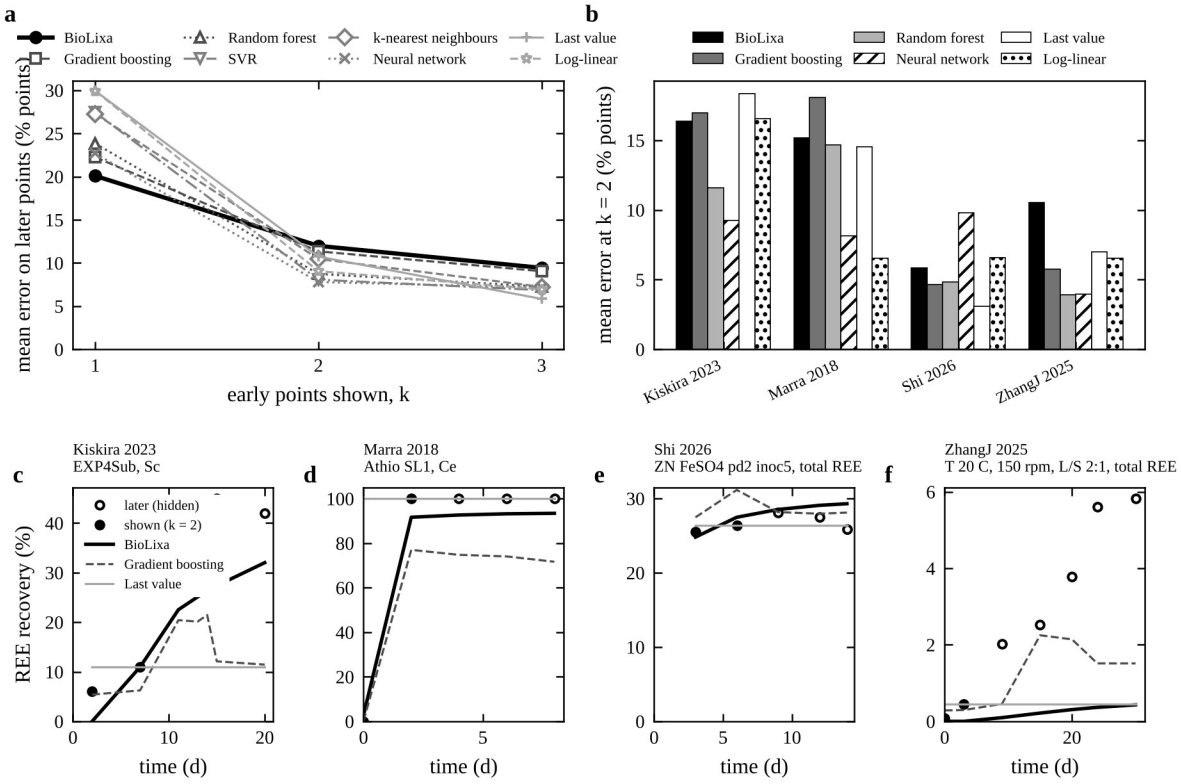


Figure 8. Held-out test, run once on four studies set aside before the model was built. (a) Mean error on the remaining points against the number k of known points. (b) Error at k = 2 for each study and method. (c to f) Examples at k = 2: filled circles are the two known points, open circles the later points.

Table 5. Mean error on the later points of a run (percentage points) with k known points, for the two assimilation schemes and the main baselines. Rehearsal: five development studies, each left out in turn. Held out: four studies set aside before the model was built; the second scheme was evaluated on them after the first.

Method	Rehearsal k = 1	k = 2	k = 3	Held out k = 1	k = 2	k = 3
BioLixa, first scheme	12.5	12.8	16.0	20.1	12.0	9.4
BioLixa, second scheme	15.1	8.9	7.9	20.3	12.2	9.0
BioLixa, first scheme with level correction	11.9	10.8	16.2	–	–	–
Last known value	15.7	7.7	6.1	29.9	10.7	5.8
Gradient boosting	12.7	9.2	8.6	22.2	11.3	9.0
Random forest	14.9	9.2	7.2	23.8	8.7	7.3
Neural network	14.9	16.5	11.1	22.7	7.8	7.2

4 Discussion

4.1 A shared model makes the published record comparable

The 17 studies compiled here were designed independently, with different organisms, residues, modes and sampling times. Even so, one parameter set described recovery and pH across the thirteen development studies to within a few percentage points and about half a pH unit. The model needed few parameters, and each has a physical meaning. They are the amount and rate of acid production of each organism group, the base released by each residue, and the places in the residue where the metal sits. With these parameters on a common scale, results from different laboratories can be compared directly. For example, a fungus that releases two thirds of the rare earths from red mud at 1 % solids and almost nothing at 5 % is the same organism in both runs. At 5 % the residue simply neutralises its acid.

4.2 What controls microbial leaching of a residue

The fitted model points to three controls, in order of importance. The first is the balance between the acid an organism makes and the base the residue releases. Leaching starts only when the acid exceeds the base capacity of the residue in the vessel. That capacity is c times the solids loading, which gives a simple estimate of the highest workable solids loading. A fungus makes about 29 mM of acid. It can overcome the base of red mud (c = 0.85 mmol g^{-1}) only below about 3 % solids. For LED lamp powder (c = 1.61 mmol g^{-1}) the limit is about 2 %. Circuit boards and cracking catalyst, with c = 0.35 and 0.30 mmol g^{-1}, allow about 8 to 10 %. Phosphogypsum releases so little base that alkalinity does not limit it in the tested range. An acidophile, which makes about 39 mM, allows a somewhat higher loading. These estimates ignore the acid used by dissolution and the time needed to make the acid, so they are upper limits. They agree with the

measured fall of recovery between 1 and 5 % solids for LED lamps (Extended Data Fig. 2b), the one development study that varied solids loading over this range with recovery measured.

The second control is where the metal sits. The host shares set the largest recovery that any acid can reach. For spent car catalyst and lamp phosphor, most of the rare earths are in no host that the acids of the development runs reach (Table 3). The model implies that for such residues more acid, a longer run or a different organism would not raise recovery much, and that a pretreatment changing the host phase would be needed. For red mud and coal fly ash, a large share is exchangeable, and a modest amount of acid releases it quickly once the alkalinity is overcome.

The third control is the type of acid. At the same dose, oxalic acid gave the lowest recovery of the four acids tested in the model, even though it gave the lowest pH of the organic acids (Fig. 5f). The reason is the loss of metal as oxalate. The model therefore suggests that organisms or culture conditions favouring citric or gluconic acid over oxalic acid suit rare earths better. Sulfuric acid from acidophiles gave a recovery similar to citric acid, but at a much lower pH, so more base would be needed to neutralise the leachate afterwards.

4.3 Relation to earlier approaches

Kinetic models fitted to single curves, such as the shrinking-core and Avrami models, describe each run slightly better than BioLixa (Table 4). Their parameters, however, belong to one run and cannot be carried to another residue or organism. Response-surface optimisation (Bahaloo-Horeh and Mousavi, 2022; Gonzalez Baez et al., 2024) finds good conditions within the ranges tested in one study, but it does not explain why those conditions work. Data-driven models trained across studies (Nguyen et al., 2025) can use many studies at once, but their inputs and outputs have no direct physical meaning. BioLixa sits between these approaches. It uses all studies at once, as a data-driven model does, and its parameters have units and meaning, as a kinetic model's do. This makes its parameters testable. The base capacity c of a residue, for example, can be measured independently by acid titration and compared with the fitted value, and the acid production of an organism can be measured in culture without residue.

4.4 What makes a run predictable

The model described the data better than it predicted them, but the two assimilation schemes show why, and how the gap closes. When only the conditions of a new run were known, the chemistry helped. BioLixa had the lowest error with one known point in the rehearsal and on the held-out studies. It knows that an alkaline residue at high solids loading will not leach and that an acidophile makes acid faster than a fungus. When two or three recovery points were known, two features of the data mattered more. First, most runs level off early. Of the 34 development runs with at least four points, 85 % reached half their final recovery within the first third of their duration. After that, a constant is a good forecast, and any model that departs from it adds error.

Second, BioLixa most needs to know how much acid the organism will still make, and recovery points alone say little about it. The second scheme tested this directly. Adding the pH measured before the second recovery point cut the rehearsal error by 30 %, and on red mud it turned the worst forecast into one better than the last value. On the held-out studies the pH data were sparse, and the gain did not appear. Taken together, the two schemes show that BioLixa forecasts well when the acid supply is observed and poorly when it must be guessed. This is a property of the data available, more than of the chemistry in the model.

The measured organic acid could not yet fill the gap (Fig. 4c), because its relation to free protons depends on the buffer of the medium, which few of the compiled studies report.

4.5 What future studies should report

Bioleaching studies would be more useful beyond their own residue if they reported a few more quantities. The most useful are the pH and the free acid over time, measured in the same vessel as the recovery. Next come the solids loading, the starting pH and the buffer of the medium, and recovery at several early times. A titration of the residue alone would give its base capacity directly. With these data the acid supply of a new run can be measured, the residue parameters of BioLixa can be carried over to new organisms and conditions, and the model can be tested more strictly than was possible here.

4.6 Practical use and computing cost

A laboratory run gives one answer per flask and takes days. In the 165 runs compiled here, the last sample was taken after a median of 9 days (interquartile range 1 to 20 days, longest 30 days), and this excludes growing the inoculum and analysing the leachate. Once fitted, BioLixa simulated one set of conditions in 0.09 s and a thousand sets in 0.18 s on a single processor core, using about 300 MB of memory (Fig. 9a, b). The fit itself is done once, on the compiled data, and needs no special hardware. A grid of organisms, residues, solids loadings, acid doses and temperatures can therefore be searched on an ordinary laptop within seconds.

The speed matters only if the answers are useful, so we checked the simplest of them, the solids-loading limit, on the held-out studies. For each held-out run we compared the acid made by its organism group, from the development fit, with the base capacity of its residue at the stated solids loading. Of the 83 series, 30 were below the limit and 53 above it. Series below the limit reached a median best recovery of 42 %, and series above it 9 % (Fig. 9c). The contrast held within each of the two studies that had runs on both sides of the limit (Kiskira et al., 2023; Zhang et al., 2025), so it is not only a difference between studies. Runs above the limit were not all failures, since 48 of the 53 series still exceeded 5 % recovery, which fits the view that the limit marks where leaching becomes poor rather than where it stops.

In practice, BioLixa can be used before laboratory work to discard conditions that the residue alkalinity rules out, to choose a solids loading and acid dose for the remaining ones, and, with the first recovery and pH measurements of a run, to judge whether the run is worth continuing. Used this way, the model can reduce the number of trial runs needed, while the experiments that remain test the conditions most likely to succeed.

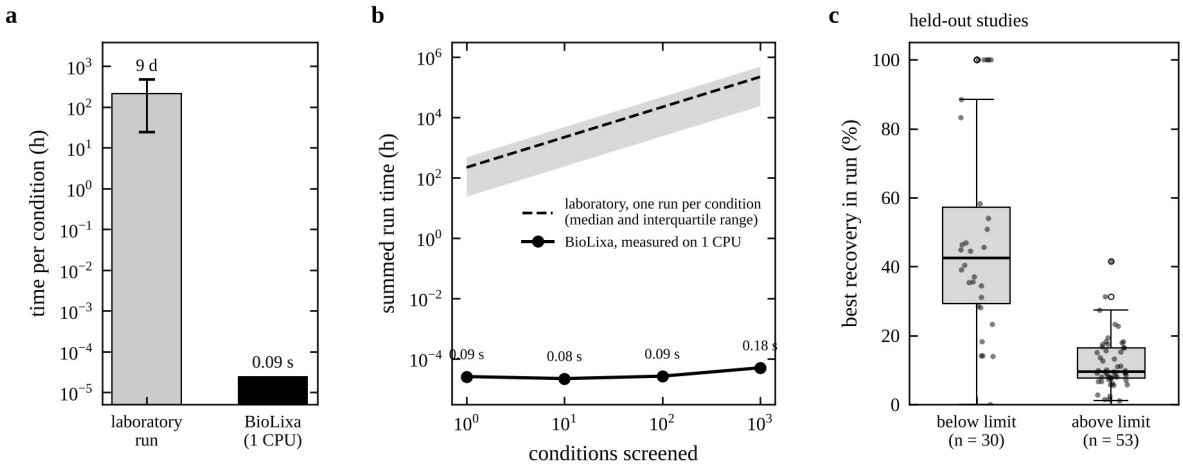


Figure 9. Computing cost and practical use. (a) Time per condition: duration of a laboratory run (median of the 165 compiled runs, bar; interquartile range, error bar) against the time BioLixa needs to simulate one condition on one processor core. (b) Summed time to screen 1 to 1000 conditions: laboratory runs, one per condition (dashed line, median; shading, interquartile range), against the measured BioLixa time. Flasks run in parallel shorten the wall time but not the summed run time. (c) Best recovery in each held-out series below and above the solids-loading limit, where the acid made by the organism group equals the base capacity of the residue. Boxes span the quartiles; points are series.

4.7 Limits

All data were extracted from published figures and tables, with digitising uncertainties of about 1 % of the axis range (Methods). The studies report different elements, often a few rare earths and not the total. Solids loading was missing for some runs of three studies and was set to 5 %. The model gives each organism group one effective acid and ignores mixed acids, the complexation constants of individual rare earths, biosorption of metal by biomass and the growth of the organism. The residue is described by host shares and rate constants fitted to leaching curves, not by measured mineralogy. The uncertainty of the group parameters (Extended Data Fig. 6) was estimated with all other parameters fixed and is a lower bound. The rehearsal covered five of the thirteen development studies, and the held-out test covered four studies. Both are small samples of organisms and residues.

4.8 From flasks to columns

All compiled experiments were stirred flasks, so the model has no transport. Acid, ligand and metal are assumed to be well mixed. In a heap, a column or a tank with settled solids, the acid must reach the grains and the released metal must move away from them. The alkaline residue around each grain can also set a local pH that differs from the bulk. BioLixa can serve as the reaction part of such a model. A next step is to couple it to a pore-scale reactive transport simulator, such as the one used by Lixa (Asgari, 2026a), so that bioleaching of residues can be designed at the scale of columns and heaps.

5 Conclusions

We compiled 17 published studies of microbial rare earth leaching from 10 industrial residues and described them with one physical model, BioLixa. The model follows the chain from acid production by

the organism, through the charge balance of the solution, to release of the metal from the solid and its loss from solution. A single parameter set reproduced 552 recovery measurements with a mean error of 2.3 percentage points and 811 pH measurements with a mean error of 0.5 pH units, across organisms, residues and laboratories.

The main finding is that the alkalinity of the residue often decides whether bioleaching works. Leaching proceeds only when the acid made by the organism exceeds the base capacity of the residue, which grows with the solids loading. For red mud, a fungus can supply enough acid only below about 3 % solids. The model also gives, for each residue, the threshold acid dose, the share of rare earths that any acid can reach, and the loss caused by oxalic acid. These quantities can be used to choose the residue, the organism and the solids loading before laboratory work begins.

As a forecasting tool, BioLixa was the most accurate of eight methods when only the conditions of a run were known, both in a development rehearsal and in four held-out studies. This makes it suited to screening residues and organisms before experiments start. It simulates a thousand sets of conditions in under a second on one processor core, whereas a single laboratory run in the compiled record took a median of 9 days. Once the first recovery points of a run were measured, its forecasts improved markedly when the early pH was assimilated as well, with a 30 % lower error in the rehearsal, which placed it ahead of all data-driven regressors. On the held-out studies, which had few early pH measurements, the gain did not appear, holding the last measured value remained a strong forecast, and the success criterion fixed in advance was not met. Accurate forecasts of single runs therefore depend on measuring pH and acid early in each run. The compiled data, the model and all scripts are released openly, so that new studies can be added and the model can be tested and extended. Coupled with transport models, BioLixa provides a basis for designing microbial recovery of rare earths from stockpiled residues at larger scales.

Data and code availability

The compiled data, with extracted values, their uncertainties and the metadata of every study, are released openly with this preprint. So are the BioLixa source code (MIT licence), the held-out protocol and the scripts that produce every number, figure and table. They are also available from the author (shahram.asgari@uga.edu), and a public repository with a permanent identifier will be listed in a later version. The original studies are cited in Table 1. Their figures and tables are not redistributed.

Competing interests

The author declares no competing interests.

References

Asgari, S.: Lixa v0.1.2: an open-source, image-informed framework for closed-loop design of leaching processes for domestic critical-mineral recovery, from the pore to the plant scale, EarthArXiv [preprint], https://doi.org/10.31223/X58F9S, 2026a.

Asgari, S.: Data-efficient prediction of rare earth leaching from industrial residues with physics-constrained machine learning, EarthArXiv [preprint], https://doi.org/10.31223/X5VR61, 2026b.

Avrami, M.: Kinetics of phase change. I. General theory, The Journal of Chemical Physics, 7, 1103–1112, https://doi.org/10.1063/1.1750380, 1939.

Baes, C. F. and Mesmer, R. E.: The Hydrolysis of Cations, Wiley, New York, 1976.

Bahaloo-Horeh, N., and Mousavi, S. M.: A novel green strategy for biorecovery of valuable elements along with enrichment of rare earth elements from activated spent automotive catalysts using fungal metabolites, Journal of Hazardous Materials, 430, 128509, https://doi.org/10.1016/j.jhazmat.2022.128509, 2022.

Barmettler, F., Castelberg, C., Fabbri, C., and Brandl, H.: Microbial mobilization of rare earth elements (REE) from mineral solids: a mini review, AIMS Microbiology, 2, 190–204, https://doi.org/10.3934/microbiol.2016.2.190, 2016.

Binnemans, K., Jones, P. T., Blanpain, B., Van Gerven, T., Yang, Y., Walton, A., and Buchert, M.: Recycling of rare earths: a critical review, Journal of Cleaner Production, 51, 1–22, https://doi.org/10.1016/j.jclepro.2012.12.037, 2013.

Borra, C. R., Pontikes, Y., Binnemans, K., and Van Gerven, T.: Leaching of rare earths from bauxite residue (red mud), Minerals Engineering, 76, 20–27, https://doi.org/10.1016/j.mineng.2015.01.005, 2015.

Brisson, V. L., Zhuang, W.-Q., and Alvarez-Cohen, L.: Bioleaching of rare earth elements from monazite sand, Biotechnology and Bioengineering, 113, 339–348, https://doi.org/10.1002/bit.25823, 2016.

Dewi, M. P., Petrus, H. T. B. M., and Okibe, N.: Recovering Secondary REE Value from Spent Oil Refinery Catalysts Using Biogenic Organic Acids, Catalysts, 10, 1090, https://doi.org/10.3390/catal10091090, 2020.

Furrer, G. and Stumm, W.: The coordination chemistry of weathering: I. Dissolution kinetics of δ-Al2O3 and BeO, Geochimica et Cosmochimica Acta, 50, 1847–1860, https://doi.org/10.1016/0016-7037(86)90243-7, 1986.

Gadd, G. M.: Metals, minerals and microbes: geomicrobiology and bioremediation, Microbiology, 156, 609–643, https://doi.org/10.1099/mic.0.037143-0, 2010.

Gelman, A., Carlin, J. B., Stern, H. S., Dunson, D. B., Vehtari, A., and Rubin, D. B.: Bayesian Data Analysis, 3rd edn., CRC Press, Boca Raton, 2013.

Gonzalez Baez, A., Muñoz, L. P., Timmermans, M. J., Garelick, H., and Purchase, D.: Molding the future: Optimization of bioleaching of rare earth elements from electronic waste by Penicillium expansum and insights into its mechanism, Bioresource Technology, 402, 130750, https://doi.org/10.1016/j.biortech.2024.130750, 2024.

Gräfe, M., Power, G., and Klauber, C.: Bauxite residue issues: III. Alkalinity and associated chemistry, Hydrometallurgy, 108, 60–79, https://doi.org/10.1016/j.hydromet.2011.02.004, 2011.

Haynes, W. M. (Ed.): CRC Handbook of Chemistry and Physics, 97th edn., CRC Press, Boca Raton, 2016.

Hopfe, S., Flemming, K., Lehmann, F., Möckel, R., Kutschke, S., and Pollmann, K.: Leaching of rare earth elements from fluorescent powder using the tea fungus Kombucha, Waste Management, 62, 211-221, https://doi.org/10.1016/j.wasman.2017.02.005, 2017.

Kingma, D. P. and Ba, J.: Adam: a method for stochastic optimization, in: 3rd International Conference on Learning Representations, San Diego, USA, arXiv:1412.6980, 2015.

Kiskira, K., Lymperopoulou, T., Lourentzatos, I., Tsakanika, L.-A., Pavlopoulos, C., Papadopoulou, K., Ochsenkühn, K.-M., Tsopelas, F., Chatzitheodoridis, E., Lyberatos, G., and Ochsenkühn-Petropoulou, M.: Bioleaching of Scandium from Bauxite Residue using Fungus Aspergillus Niger, Waste and Biomass Valorization, 14, 3377-3390, https://doi.org/10.1007/s12649-023-02116-5, 2023.

Levenspiel, O.: Chemical Reaction Engineering, 3rd edn., Wiley, New York, 1999.

MacKay, D. J. C.: A practical Bayesian framework for backpropagation networks, Neural Computation, 4, 448–472, https://doi.org/10.1162/neco.1992.4.3.448, 1992.

Marra, A., Cesaro, A., Rene, E. R., Belgiorno, V., and Lens, P. N.: Bioleaching of metals from WEEE shredding dust, Journal of Environmental Management, 210, 180-190, https://doi.org/10.1016/j.jenvman.2017.12.066, 2018.

Moldoveanu, G. A. and Papangelakis, V. G.: Recovery of rare earth elements adsorbed on clay minerals: I. Desorption mechanism, Hydrometallurgy, 117–118, 71–78, https://doi.org/10.1016/j.hydromet.2012.02.007, 2012.

Nadi, S., Pourhossein, F., and Mousavi, S. M.: Sustainable bio-extraction of rare earth elements from discarded LED lamps, Scientific Reports, 15, 21655, https://doi.org/10.1038/s41598-025-04937-x, 2025.

Nguyen, Q. L., Lai, H. N., Nguyen, H. T. M., Pham, L. L., Herdean, A., Poddar, N., Kuzhiumparambil, U., Nguyen, A., Pernice, M., Ralph, P. J., and Vo, P. H. N.: Explainable artificial intelligence for predicting rare earth elements leaching from secondary resources, Journal of Hazardous Materials, 496, 139479, https://doi.org/10.1016/j.jhazmat.2025.139479, 2025.

Park, S., and Liang, Y.: Bioleaching of trace elements and rare earth elements from coal fly ash, International Journal of Coal Science & Technology, 6, 74-83, https://doi.org/10.1007/s40789-019-0238-5, 2019.

Paszke, A., Gross, S., Massa, F., Lerer, A., Bradbury, J., Chanan, G., Killeen, T., Lin, Z., Gimelshein, N., Antiga, L., Desmaison, A., Köpf, A., Yang, E., DeVito, Z., Raison, M., Tejani, A., Chilamkurthy, S., Steiner, B., Fang, L., Bai, J., and Chintala, S.: PyTorch: an imperative style, high-performance deep learning library, in: Advances in Neural Information Processing Systems 32, 8024–8035, 2019.

Pedram, H., Hosseini, M. R., and Bahrami, A.: Utilization of A. niger strains isolated from pistachio husk and grape skin in the bioleaching of valuable elements from red mud, Hydrometallurgy, 198, 105495, https://doi.org/10.1016/j.hydromet.2020.105495, 2020.

Pedregosa, F., Varoquaux, G., Gramfort, A., Michel, V., Thirion, B., Grisel, O., Blondel, M., Prettenhofer, P., Weiss, R., Dubourg, V., Vanderplas, J., Passos, A., Cournapeau, D., Brucher, M., Perrot, M., and Duchesnay, É.: Scikit-learn: machine learning in Python, Journal of Machine Learning Research, 12, 2825–2830, 2011.

Qu, Y., and Lian, B.: Bioleaching of rare earth and radioactive elements from red mud using Penicillium tricolor RM-10, Bioresource Technology, 136, 16-23, https://doi.org/10.1016/j.biortech.2013.03.070, 2013.

Qu, Y., Li, H., Wang, X., Tian, W., Shi, B., Yao, M., and Zhang, Y.: Bioleaching of Major, Rare Earth, and Radioactive Elements from Red Mud by using Indigenous Chemoheterotrophic Bacterium Acetobacter sp., Minerals, 9, 67, https://doi.org/10.3390/min9020067, 2019.

Reed, D. W., Fujita, Y., Daubaras, D. L., Jiao, Y., and Thompson, V. S.: Bioleaching of rare earth elements from waste phosphors and cracking catalysts, Hydrometallurgy, 166, 34-40, https://doi.org/10.1016/j.hydromet.2016.08.006, 2016.

Sawyer, D. T.: Metal-gluconate complexes, Chemical Reviews, 64, 633–643, https://doi.org/10.1021/cr60232a003, 1964.

Shi, S., Chen, T., and Ren, S.: Recovery of Rare Earth Elements from Different Types of Coal Fly Ash by Direct Bioleaching, Materials, 19, 2861, https://doi.org/10.3390/ma19132861, 2026.

Stumm, W. and Morgan, J. J.: Aquatic Chemistry: Chemical Equilibria and Rates in Natural Waters, 3rd edn., Wiley, New York, 1996.

Taggart, R. K., Hower, J. C., Dwyer, G. S., and Hsu-Kim, H.: Trends in the rare earth element content of U.S.-based coal combustion fly ashes, Environmental Science & Technology, 50, 5919–5926, https://doi.org/10.1021/acs.est.6b00085, 2016.

U.S. Geological Survey: Mineral Commodity Summaries 2025, U.S. Geological Survey, Reston, VA, https://doi.org/10.3133/mcs2025, 2025.

Zhang, D.-R., Chen, H.-R., Xia, J.-L., Nie, Z.-Y., Zhang, R.-Y., and Pakostova, E.: Efficient dealkalization of red mud and recovery of valuable metals by a sulfur-oxidizing bacterium, Frontiers in Microbiology, 13, 973568, https://doi.org/10.3389/fmicb.2022.973568, 2022.

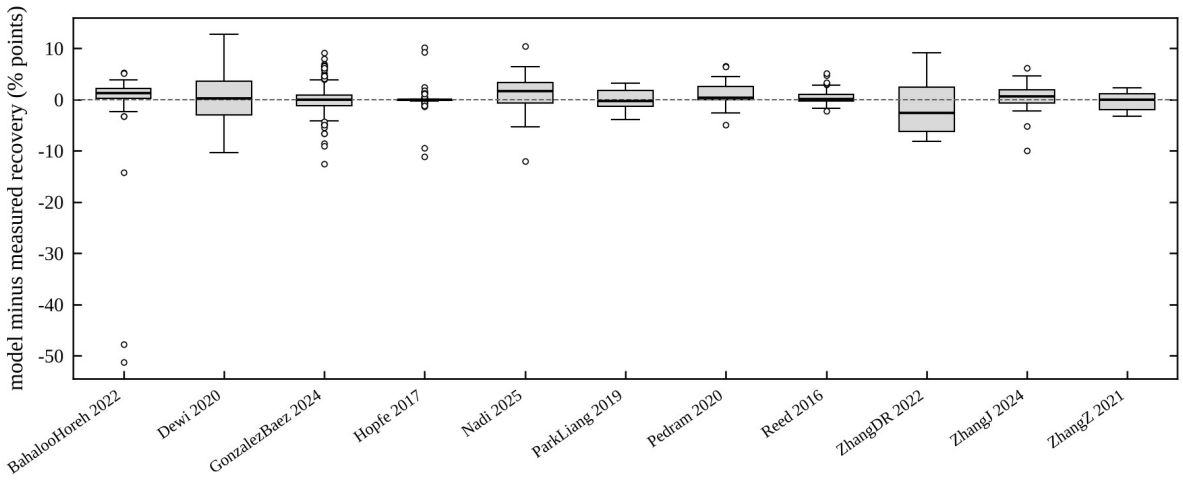
Zhang, J., Qi, Z., He, Z., Zhang, X., Zhang, Q., and Su, X.: Study on the Extraction of Rare Earth Elements (REEs) from Phosphogypsum Using Gluconobacter oxydans Culture Solution, Molecules, 30, 674, https://doi.org/10.3390/molecules30030674, 2025.

Zhang, J., Zhang, X., Su, X., Du, H., Lu, Y., and Zhang, Q.: Rare Earth Extraction from Phosphogypsum by Aspergillus niger Culture Broth, Molecules, 29, 1266, https://doi.org/10.3390/molecules29061266, 2024.

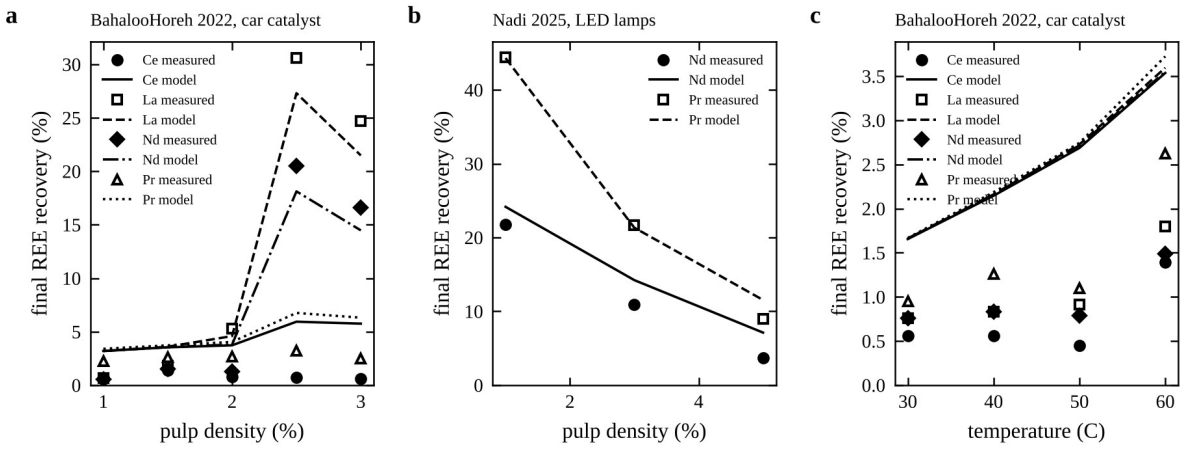
Zhang, Z., Allen, L., Podder, P., Free, M. L., and Sarswat, P. K.: Recovery and Enhanced Upgrading of Rare Earth Elements from Coal-Based Resources: Bioleaching and Precipitation, Minerals, 11, 484, https://doi.org/10.3390/min11050484, 2021.

Zwietering, M. H., Jongenburger, I., Rombouts, F. M., and van 't Riet, K.: Modeling of the bacterial growth curve, Applied and Environmental Microbiology, 56, 1875–1881, https://doi.org/10.1128/aem.56.6.1875-1881.1990, 1990.

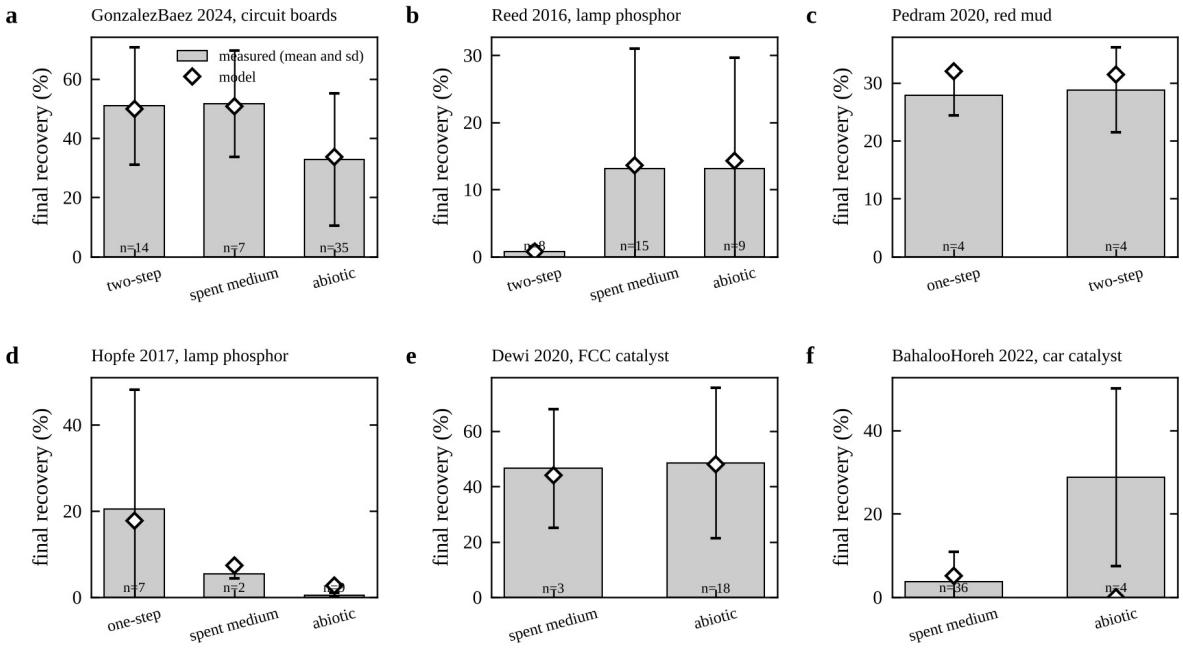
Extended Data



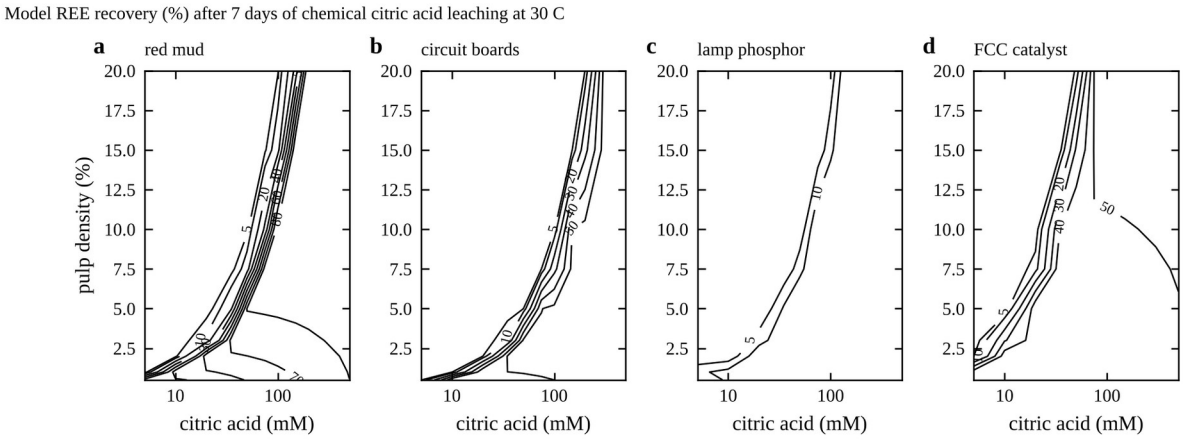
Extended Data Fig. 1. Recovery residuals (model minus measured) of the development fit for each study. Boxes span the quartiles, whiskers 1.5 times the interquartile range.



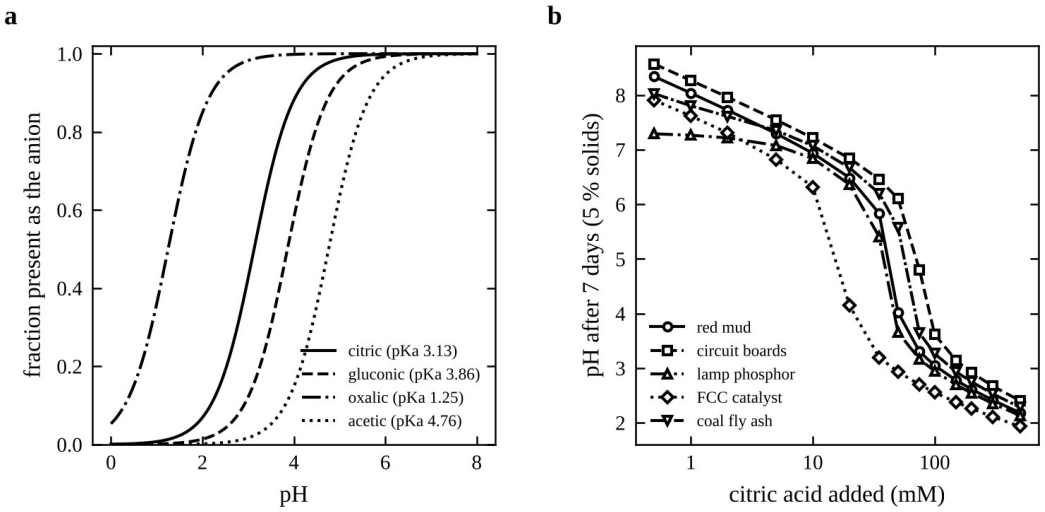
Extended Data Fig. 2. Measured (symbols) and fitted (lines) final recovery against solids loading and temperature. (a) Spent medium of Aspergillus niger on car catalyst at 60 °C (Bahaloo-Horeh and Mousavi, 2022). (b) Spent medium of Acidithiobacillus thiooxidans on LED lamps (Nadi et al., 2025). (c) As (a), at 1.5 % solids and four temperatures.



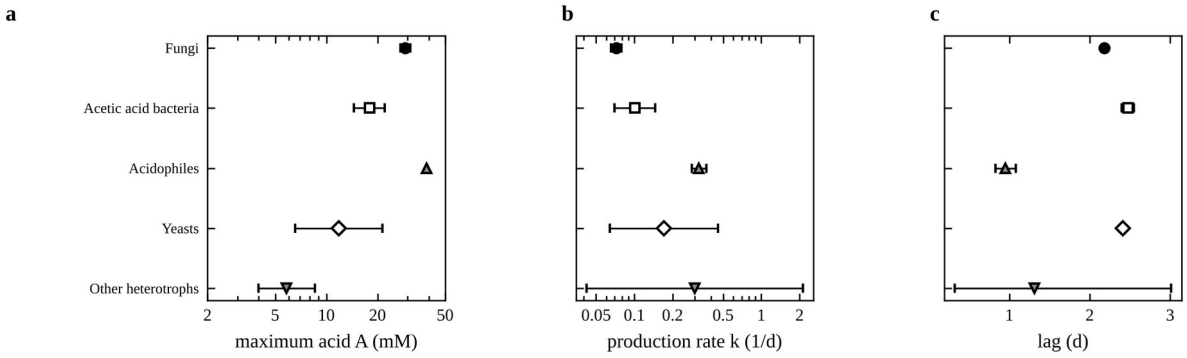
Extended Data Fig. 3. Final recovery by leaching mode in six development studies. Bars are the measured mean and standard deviation over runs and elements, diamonds the model; n is the number of series.



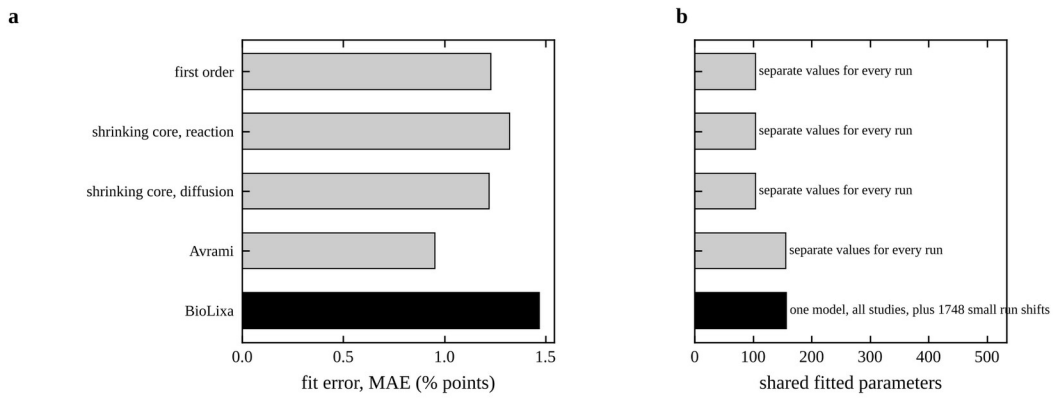
Extended Data Fig. 4. Model response surfaces: recovery after 7 days of chemical citric acid leaching at 30 °C against acid dose and solids loading, for four residues. Contours in percent.



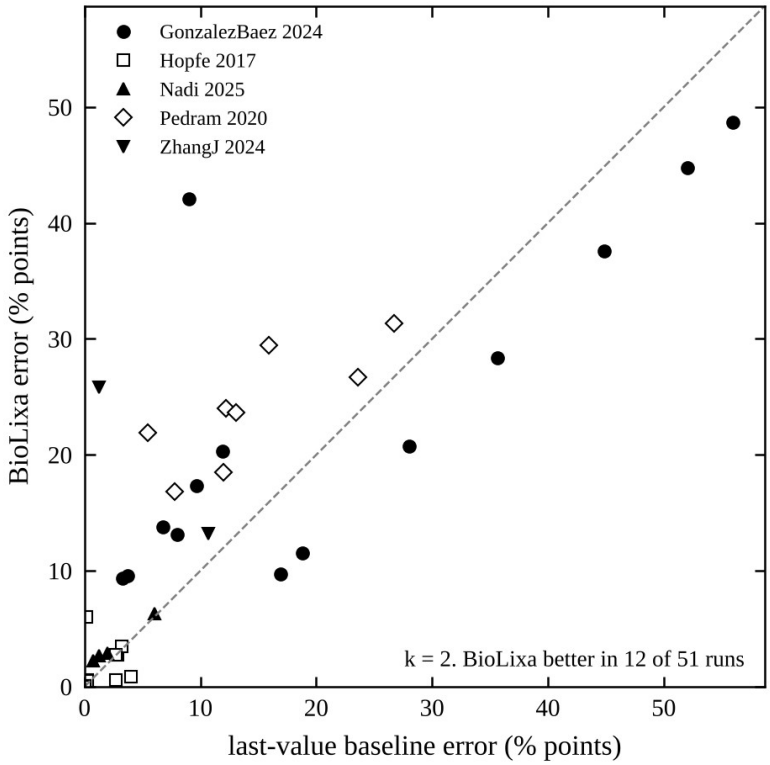
Extended Data Fig. 5. Solution chemistry in the model. (a) Fraction of each acid present as the anion against pH, from the constants of Extended Data Table 1. (b) pH after 7 days against the dose of chemical citric acid at 5 % solids for five residues, with the fitted alkalinity and acid use.



Extended Data Fig. 6. Fitted acid production of each organism group with approximate 95 % intervals from the curvature of the loss, computed with all other parameters fixed (a lower bound on the uncertainty). (a) Largest acid amount, (b) production rate, (c) lag.



Extended Data Fig. 7. BioLixa and four kinetic models fitted run by run, on the same recovery points. (a) Mean absolute error. (b) Number of fitted parameters; BioLixa also has run shifts pulled towards zero.



Extended Data Fig. 8. Development rehearsal, run by run at k = 2: error of BioLixa against the error of holding the last known value. Points above the dashed line are runs where the last value was better.

Extended Data Table 1. Acid constants used in the charge balance, at 25 °C. Organic acids are represented by their first dissociation constant, from the CRC Handbook (Haynes, 2016) except gluconic acid (Sawyer, 1964). The organic acid mix is given an effective value (this work). Strong acids are given a very low pKa so that they are fully dissociated.

Acid	Effective pKa	Protons counted	Complexing ligand	Oxalate
citric	3.13	1.0	yes	no
gluconic	3.86	1.0	yes	no
oxalic	1.25	1.0	yes	yes
lactic	3.86	1.0	yes	no
succinic	4.21	1.0	yes	no
acetic	4.76	1.0	no	no
organic acid mix	3.7	1.0	yes	no
sulfuric	-3.0	2.0	no	no
hydrochloric	-6.0	1.0	no	no

Extended Data Table 2. Fitted quantities of BioLixa, the level at which each is shared, and its prior. N(m, s): normal with mean m and standard deviation s on the scale given.

Symbol	Meaning	Unit	Level	Prior
A	maximum acid made by the organism	mM (proton equivalents)	organism group, run shift	log A ~ N(log A_0, 1); A_0 = 60 fungi and acetic, 150 acidophiles, 20 yeasts, 10 heterotrophs
k	acid production rate	1/d	organism group	log k ~ N(log 0.3, 1)
lag	time before acid production starts	d	organism group, run shift	softplus argument ~ N(1, 1)
t_{pre}	pre-growth time in two-step runs	d	organism group	softplus argument ~ N(3, 1)
f_{ox}	oxalate fraction of the biogenic acid	-	organism group	logit ~ N(-2, 1) fungi, N(-6, 1) others
c	alkalinity of the waste	mmol per g	waste and element class, run shift	log c ~ N(log 0.5, 2)
k_B	rate of alkalinity release	1/d	waste and element class	log k_B ~ N(0, 2)
c_{mat}	acid used up by the dissolving host	mmol per g	waste and element class	log c_{mat} ~ N(log 0.5, 2)
s_0 to s_3	REE shares: exchangeable, acid-soluble, diffusion-limited, locked	-	waste and element class, series shift	softmax logits ~ N(0, 2)
k_{r0}	acid-soluble host rate constant	1/d	waste and element class, run shift	log k_{r0} ~ N(2, 3)
n	reaction order in H+	-	waste and element class	0.3 + 1.2 sigmoid(z), z ~ N(0, 1)
k_{d0}	diffusion-limited host rate constant	1/d	waste and element class	log k_{d0} ~ N(0, 3)
K_{ex}	exchange constant	L/mol	waste and element class	log K_{ex} ~ N(3, 2)

Symbol	Meaning	Unit	Level	Prior
κ	ligand strength in the dissolution rate	-	global	$\log \kappa \sim N(0, 3)$
κ_x	ligand strength in exchange	-	global	$\log \kappa_x \sim N(0, 3)$
θ	largest fraction lost to oxalate precipitation	-	global	$\text{logit} \sim N(0, 2)$
K_{ox}	free oxalate at half of the largest loss	mol/L	global	$\log K_{ox} \sim N(\log 0.001, 2)$
pH_p	pH where hydrolysis losses reach half	-	global	$N(6.5, 1)$
E_a	apparent activation energy	kJ/mol	global	$N(40, 15)$

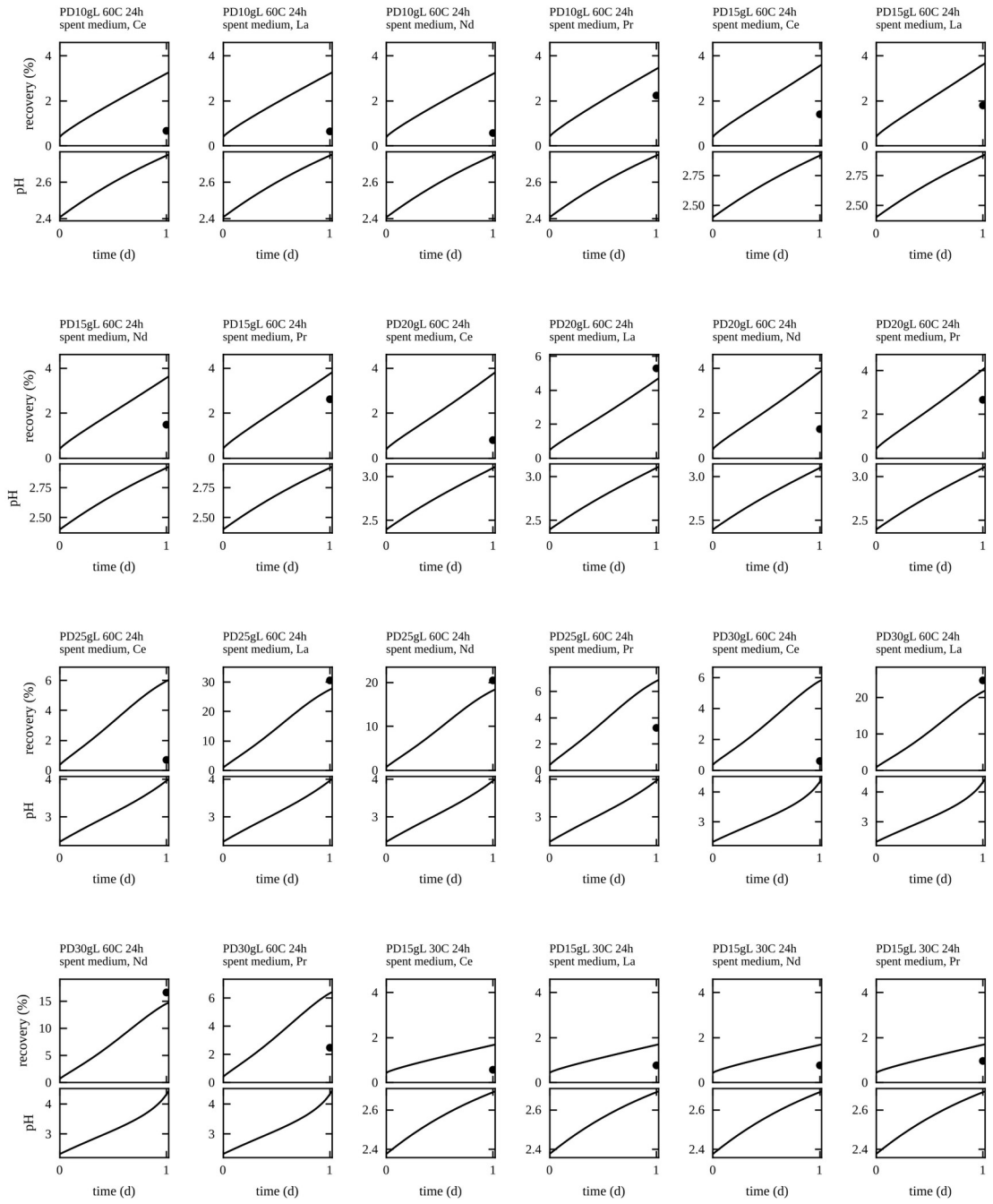
Supplementary Information

Residue alkalinity limits microbial leaching of rare earth elements from industrial wastes

Shahram Asgari, Department of Marine Sciences, University of Georgia (shahram.asgari@uga.edu)

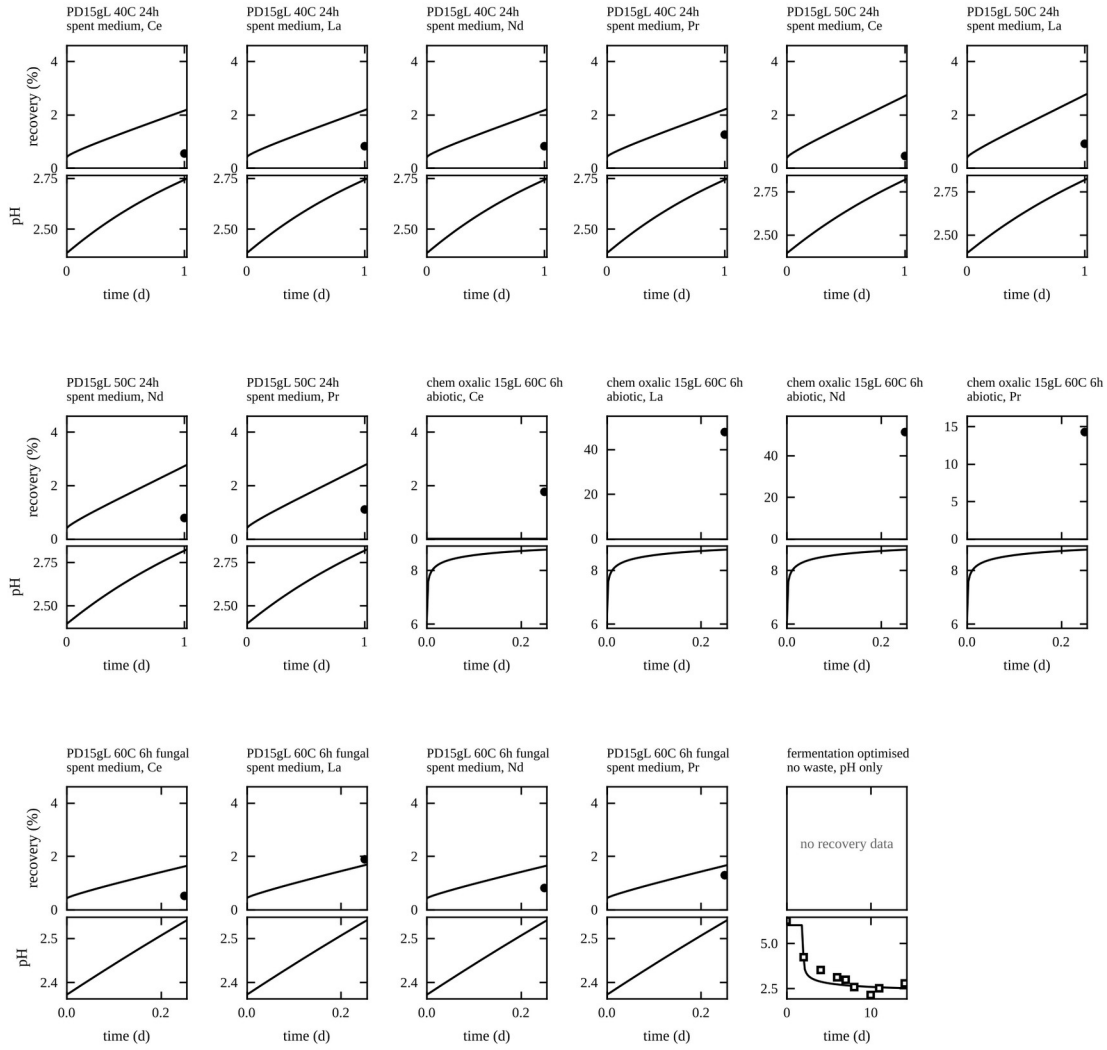
Supplementary Figs S1 to S13 show every development run fitted by BioLixa, one figure per study. Each panel pair is one series: rare earth recovery above and pH below, on the same time axis. Lines are the model with the development parameters, symbols the extracted measurements. The panel title gives the run name used in the original paper, the leaching mode and the element. Runs that report pH but no recovery are shown with an empty recovery panel.

Supplementary Fig. S1 | BahalooHoreh 2022, car catalyst (part 1). Each panel pair is one run: recovery above, pH below. Lines: fitted model; symbols: measured.



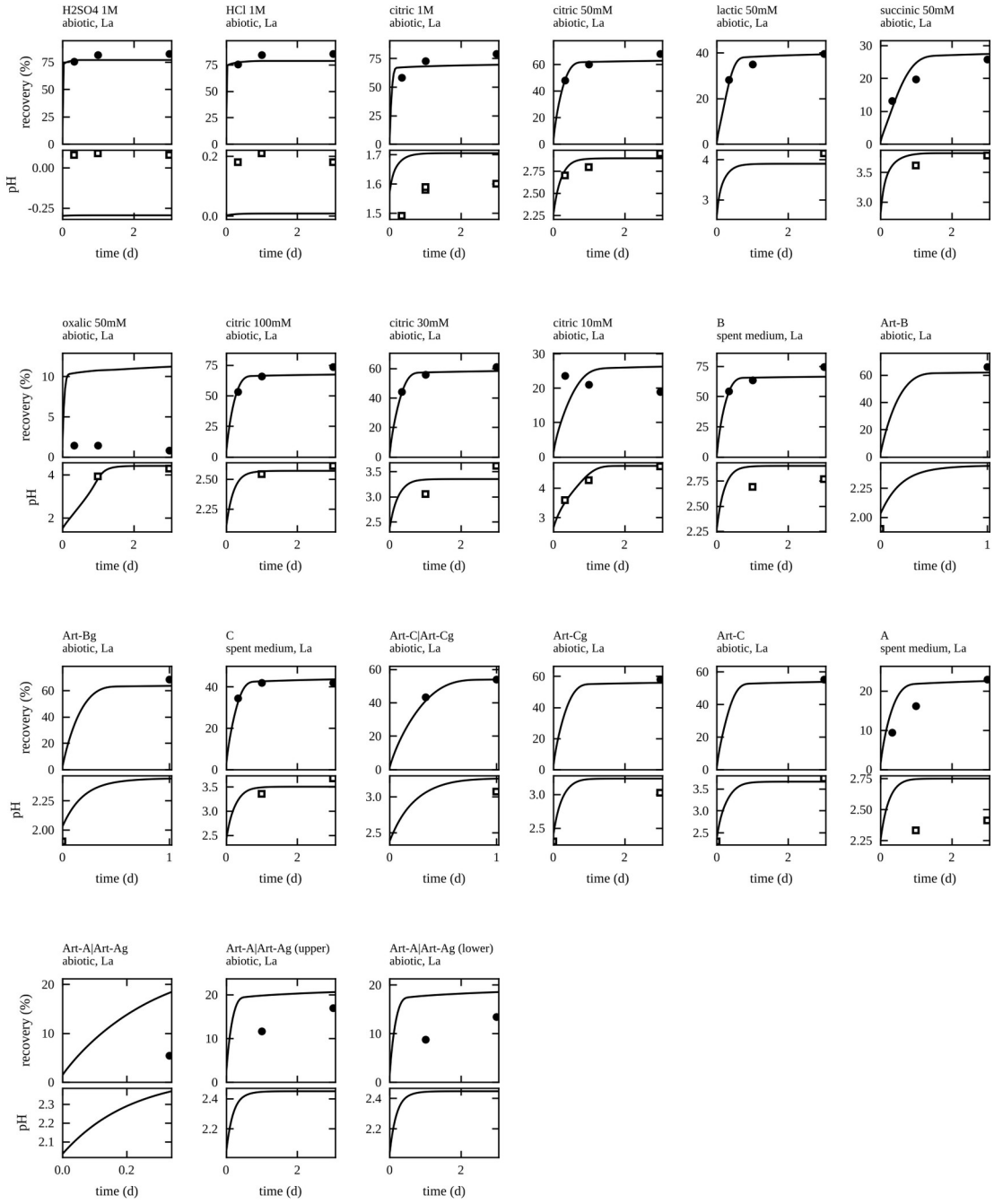
Supplementary Fig. S1 (part 1 of 2). Bahaloo-Horeh and Mousavi (2022): fitted development runs. Each panel pair is one series, recovery above and pH below. Lines, model; symbols, measured.

Supplementary Fig. S1 | BahalooHoreh 2022, car catalyst (part 2). Each panel pair is one run: recovery above, pH below. Lines: fitted model; symbols: measured.



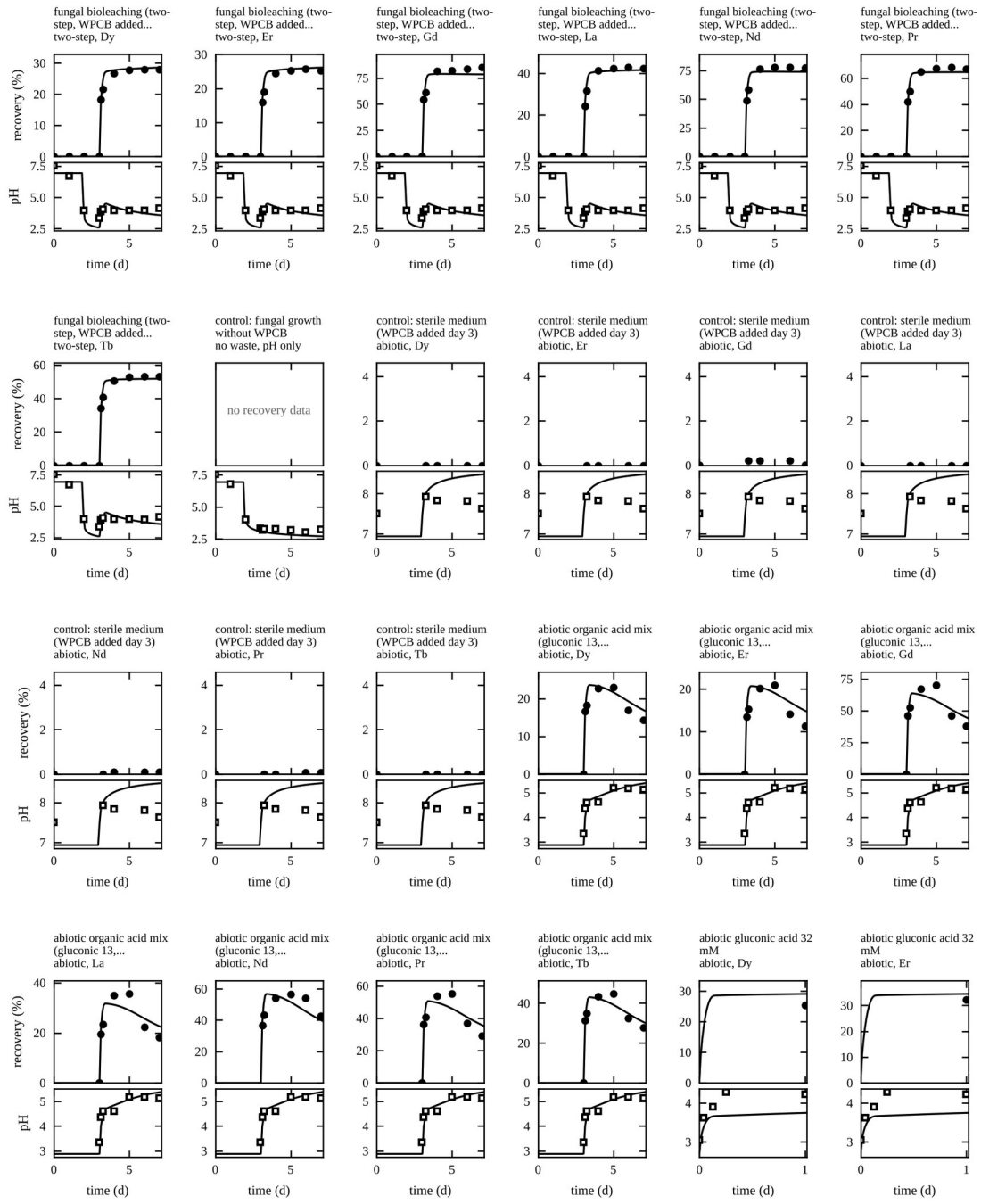
Supplementary Fig. S1 (part 2 of 2). Bahaloo-Horeh and Mousavi (2022): fitted development runs. Each panel pair is one series, recovery above and pH below. Lines, model; symbols, measured.

Supplementary Fig. S2 | Dewi 2020, FCC catalyst. Each panel pair is one run: recovery above, pH below. Lines: fitted model; symbols: measured.



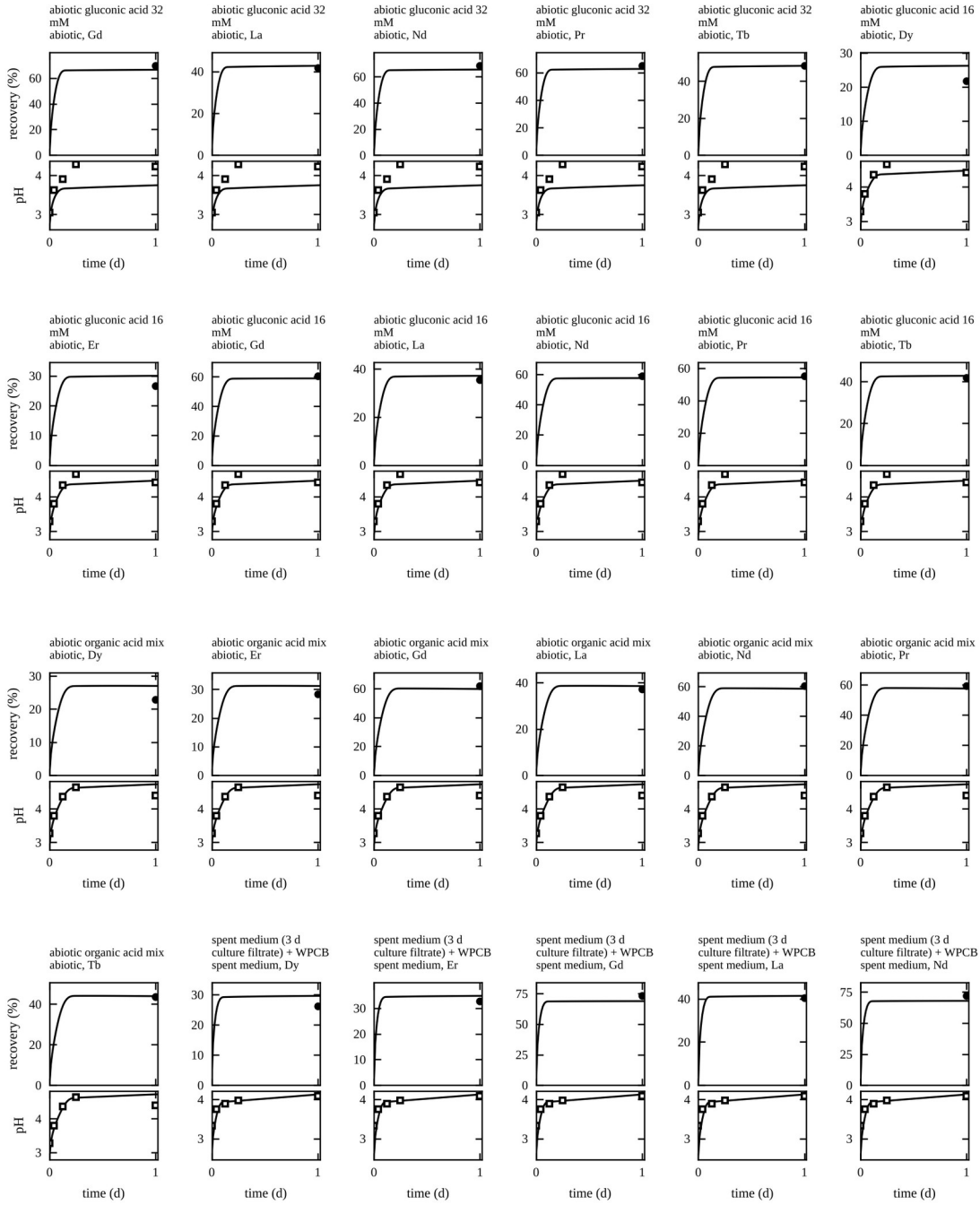
Supplementary Fig. S2. Dewi et al. (2020): fitted development runs. Each panel pair is one series, recovery above and pH below. Lines, model; symbols, measured.

Supplementary Fig. S3 | GonzalezBaez 2024, circuit boards (part 1). Each panel pair is one run: recovery above, pH below. Lines: fitted model; symbols: measured.



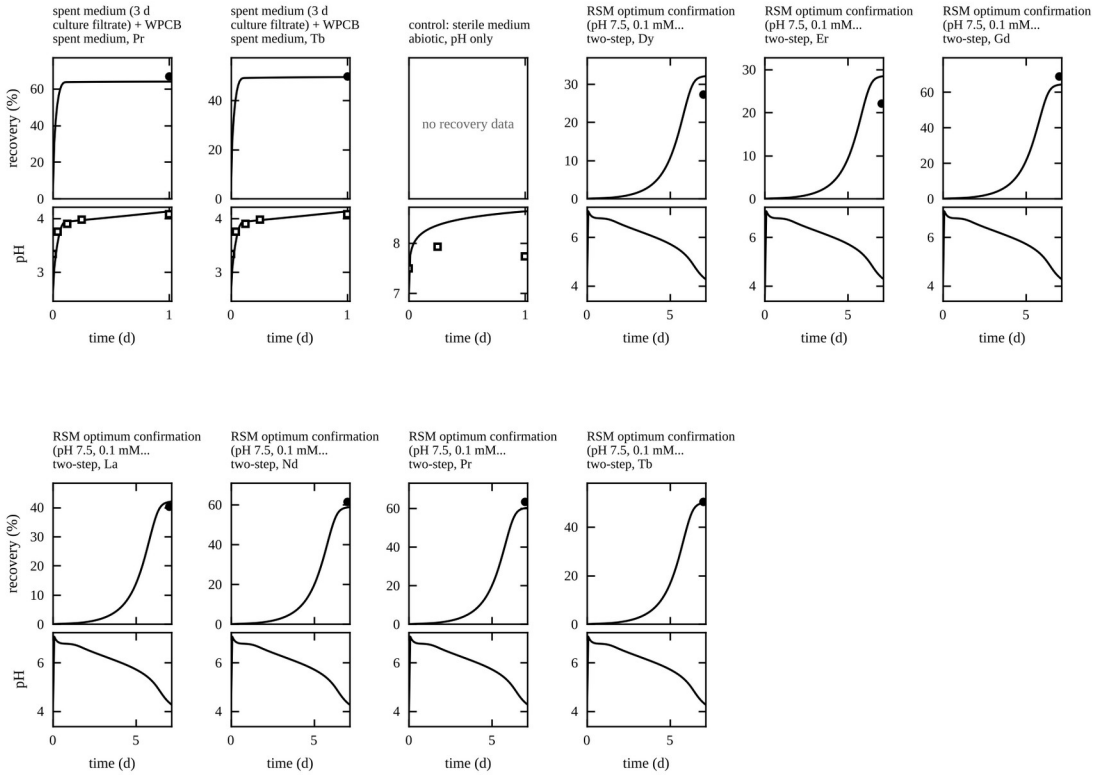
Supplementary Fig. S3 (part 1 of 3). Gonzalez Baez et al. (2024): fitted development runs. Each panel pair is one series, recovery above and pH below. Lines, model; symbols, measured.

Supplementary Fig. S3 | GonzalezBaez 2024, circuit boards (part 2). Each panel pair is one run: recovery above, pH below. Lines: fitted model; symbols: measured.



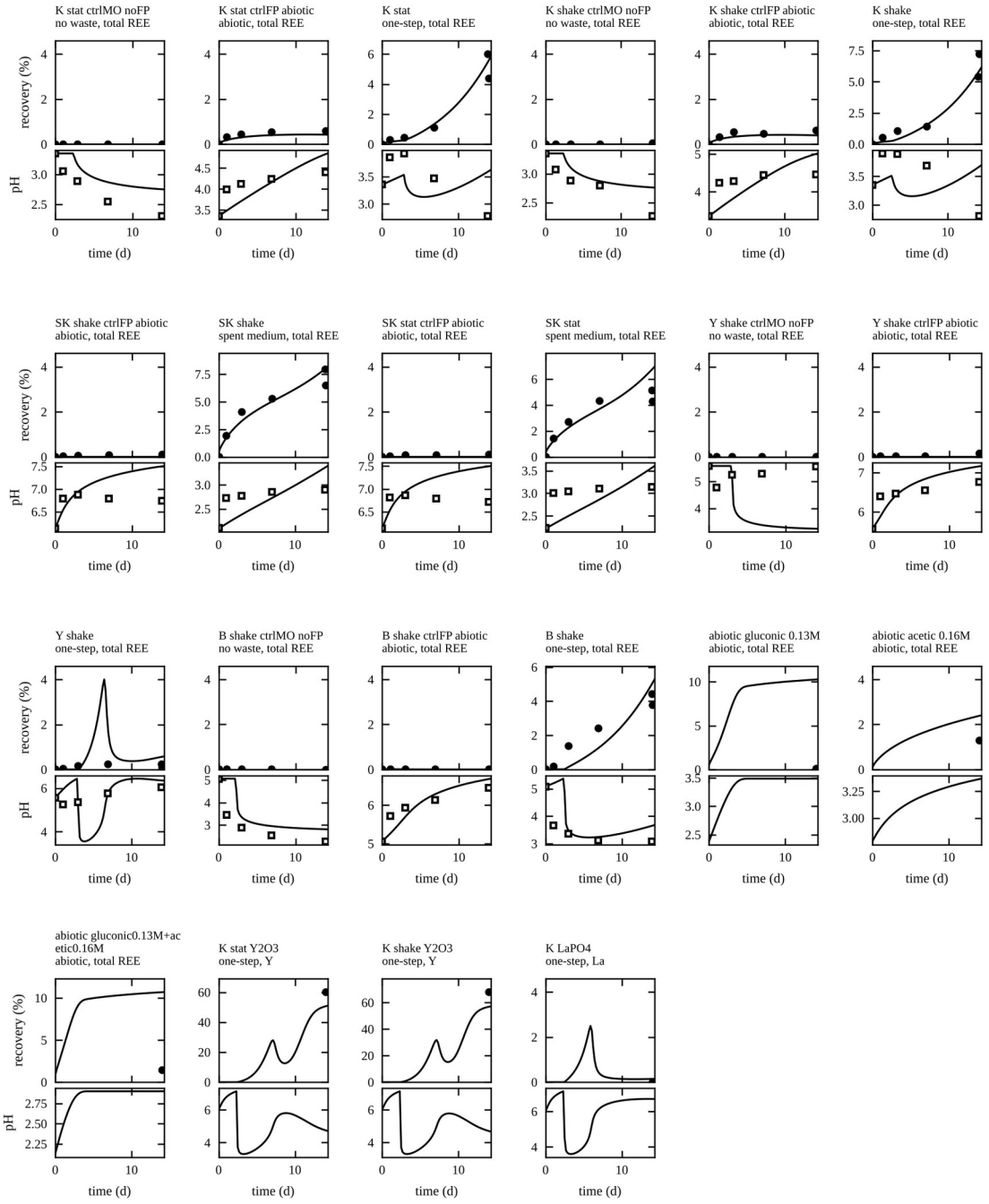
Supplementary Fig. S3 (part 2 of 3). Gonzalez Baez et al. (2024): fitted development runs. Each panel pair is one series, recovery above and pH below. Lines, model; symbols, measured.

Supplementary Fig. S3 | GonzalezBaez 2024, circuit boards (part 3). Each panel pair is one run: recovery above, pH below. Lines: fitted model; symbols: measured.



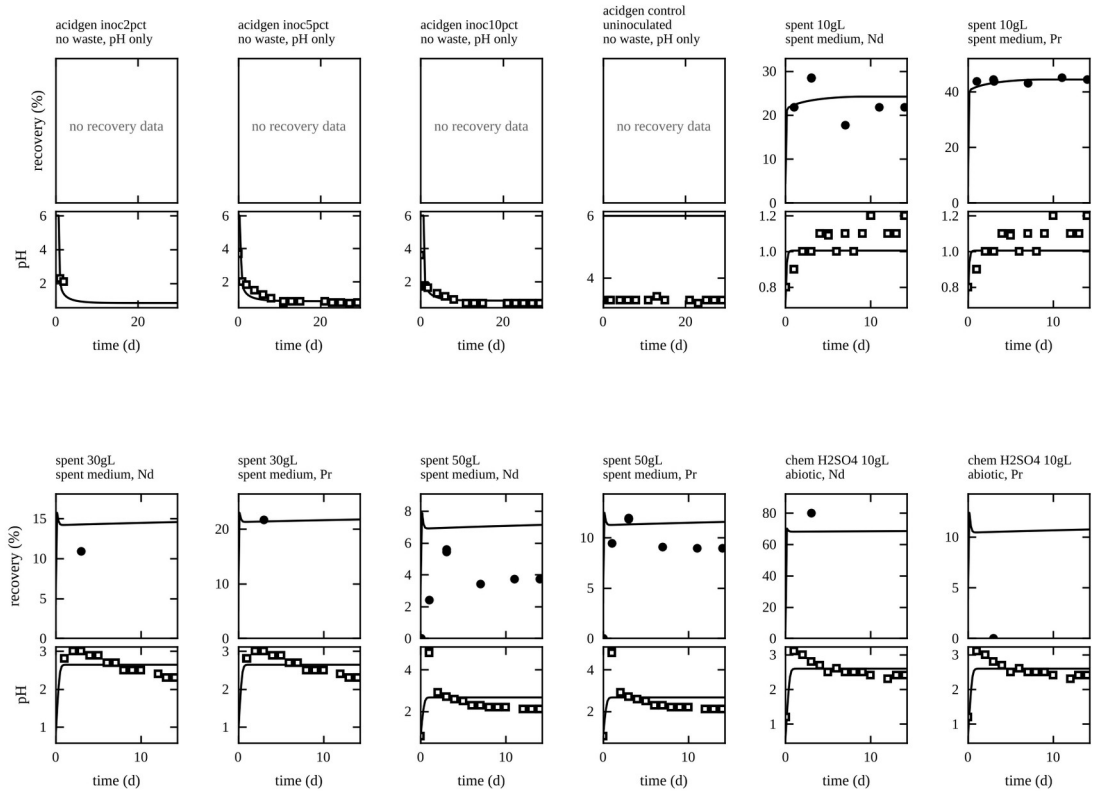
Supplementary Fig. S3 (part 3 of 3). Gonzalez Baez et al. (2024): fitted development runs. Each panel pair is one series, recovery above and pH below. Lines, model; symbols, measured.

Supplementary Fig. S4 | Hopfe 2017, lamp phosphor. Each panel pair is one run: recovery above, pH below. Lines: fitted model; symbols: measured.



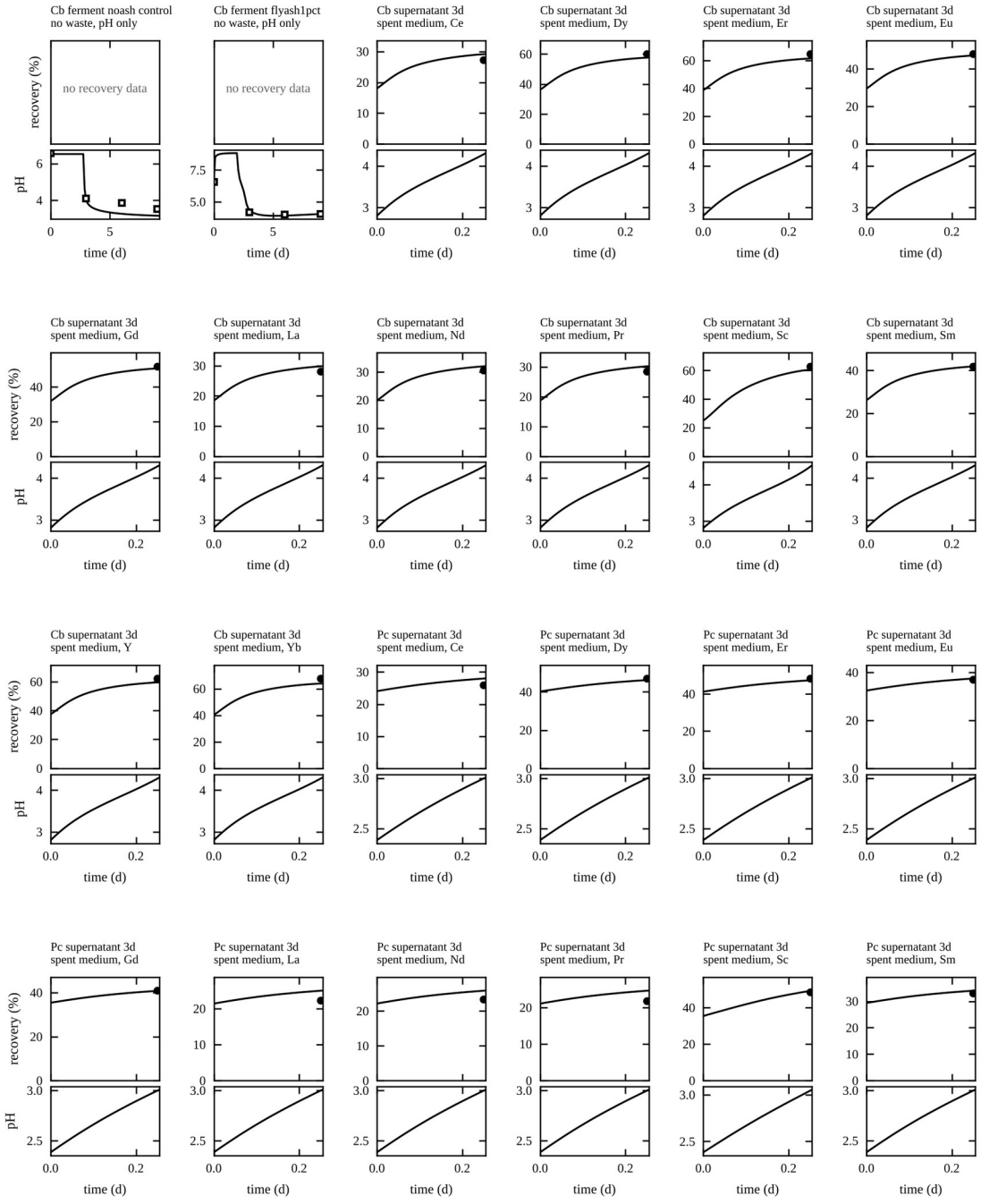
Supplementary Fig. S4. Hopfe et al. (2017): fitted development runs. Each panel pair is one series, recovery above and pH below. Lines, model; symbols, measured.

Supplementary Fig. S5 | Nadi 2025, LED lamps. Each panel pair is one run: recovery above, pH below. Lines: fitted model; symbols: measured.



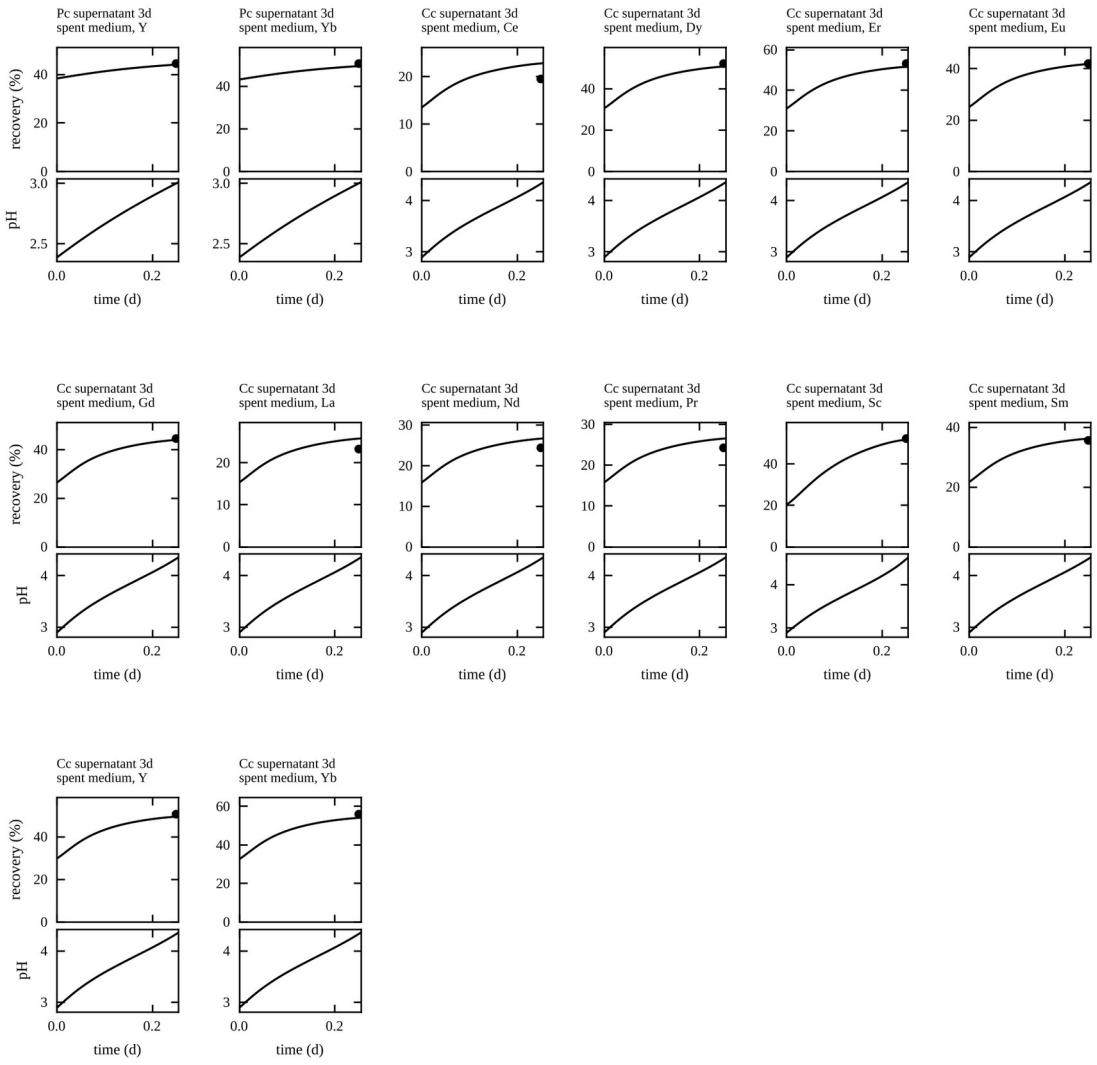
Supplementary Fig. S5. Nadi et al. (2025): fitted development runs. Each panel pair is one series, recovery above and pH below. Lines, model; symbols, measured.

Supplementary Fig. S6 | ParkLiang 2019, coal fly ash (part 1). Each panel pair is one run: recovery above, pH below. Lines: fitted model; symbols: measured.



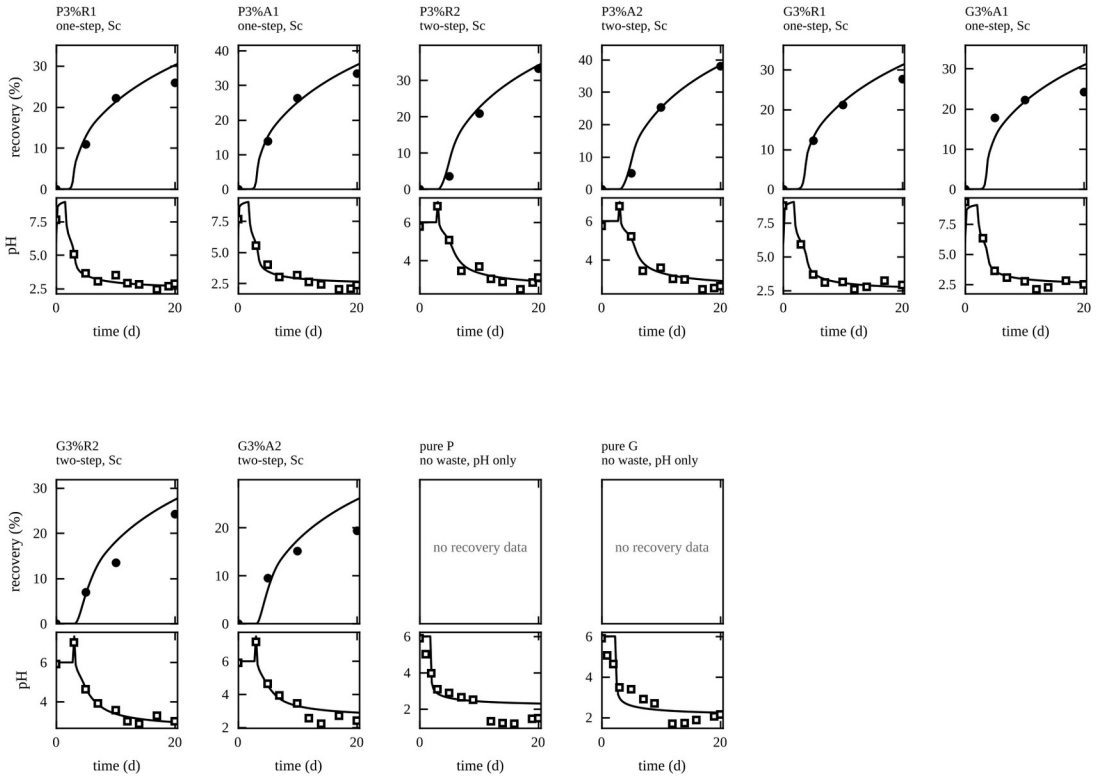
Supplementary Fig. S6 (part 1 of 2). Park and Liang (2019): fitted development runs. Each panel pair is one series, recovery above and pH below. Lines, model; symbols, measured.

Supplementary Fig. S6 | ParkLiang 2019, coal fly ash (part 2). Each panel pair is one run: recovery above, pH below. Lines: fitted model; symbols: measured.



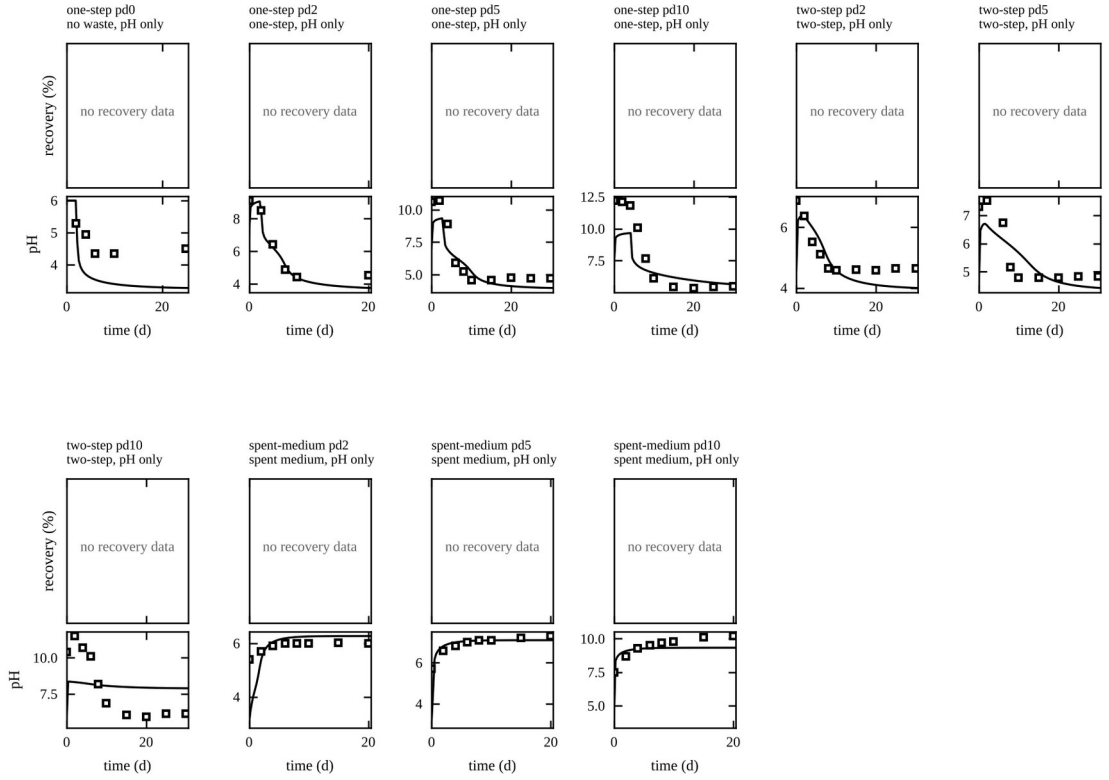
Supplementary Fig. S6 (part 2 of 2). Park and Liang (2019): fitted development runs. Each panel pair is one series, recovery above and pH below. Lines, model; symbols, measured.

Supplementary Fig. S7 | Pedram 2020, red mud. Each panel pair is one run: recovery above, pH below. Lines: fitted model; symbols: measured.



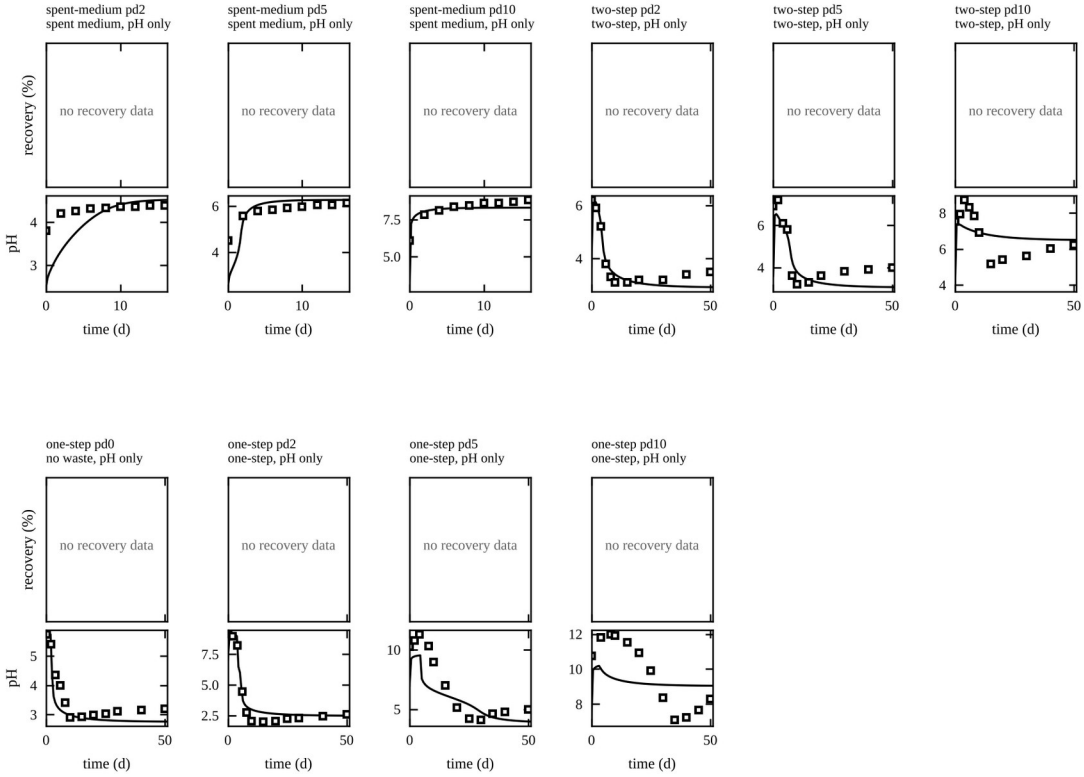
Supplementary Fig. S7. Pedram et al. (2020): fitted development runs. Each panel pair is one series, recovery above and pH below. Lines, model; symbols, measured.

Supplementary Fig. S8 | Qu 2019, red mud. Each panel pair is one run: recovery above, pH below. Lines: fitted model; symbols: measured.



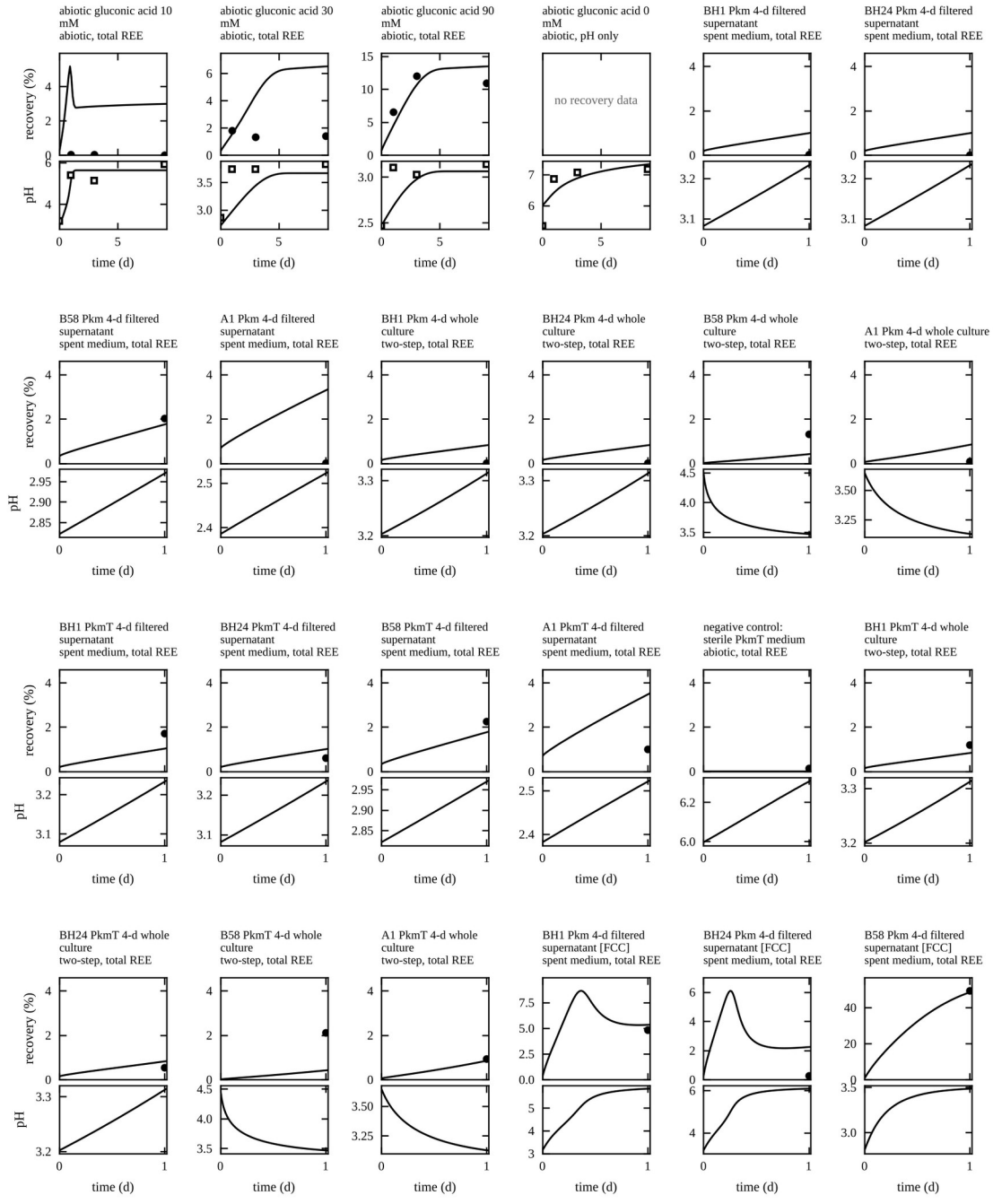
Supplementary Fig. S8. Qu et al. (2019): fitted development runs. Each panel pair is one series, recovery above and pH below. Lines, model; symbols, measured.

Supplementary Fig. S9 | QuLian 2013, red mud. Each panel pair is one run: recovery above, pH below. Lines: fitted model; symbols: measured.



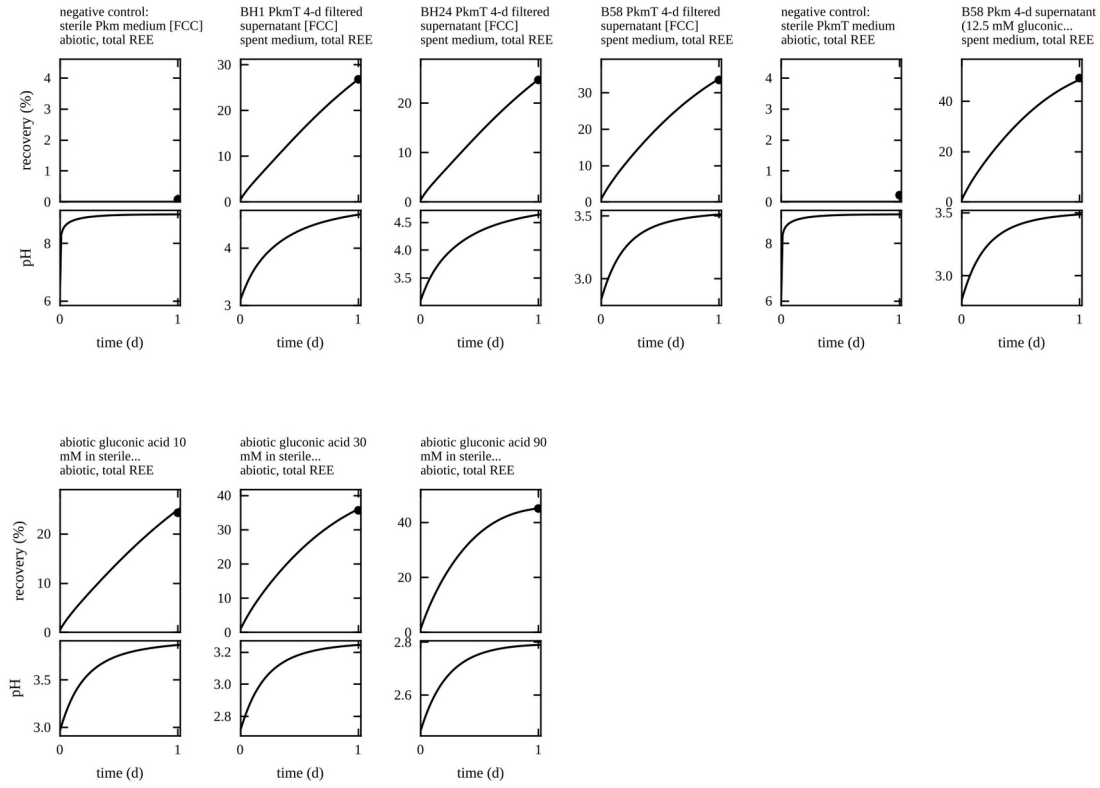
Supplementary Fig. S9. Qu and Lian (2013): fitted development runs. Each panel pair is one series, recovery above and pH below. Lines, model; symbols, measured.

Supplementary Fig. S10 | Reed 2016, lamp phosphor (part 1). Each panel pair is one run: recovery above, pH below. Lines: fitted model; symbols: measured.



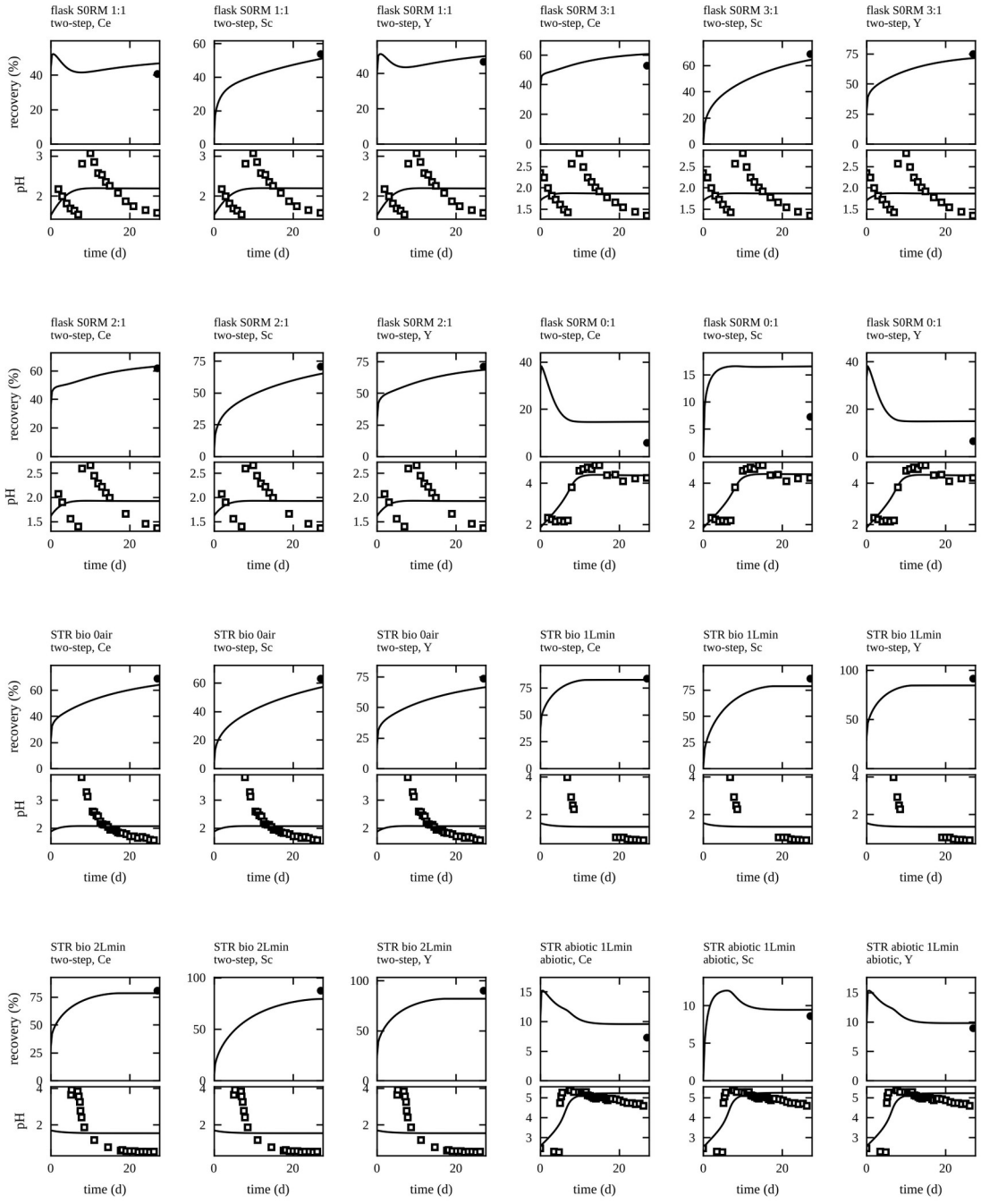
Supplementary Fig. S10 (part 1 of 2). Reed et al. (2016): fitted development runs. Each panel pair is one series, recovery above and pH below. Lines, model; symbols, measured.

Supplementary Fig. S10 | Reed 2016, FCC catalyst (part 2). Each panel pair is one run: recovery above, pH below. Lines: fitted model; symbols: measured.



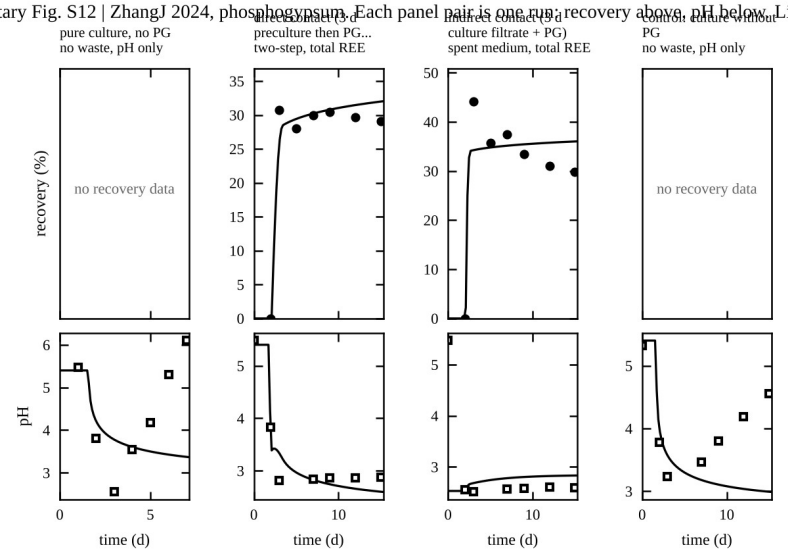
Supplementary Fig. S10 (part 2 of 2). Reed et al. (2016): fitted development runs. Each panel pair is one series, recovery above and pH below. Lines, model; symbols, measured.

Supplementary Fig. S11 | ZhangDR 2022, red mud. Each panel pair is one run: recovery above, pH below. Lines: fitted model; symbols: measured.



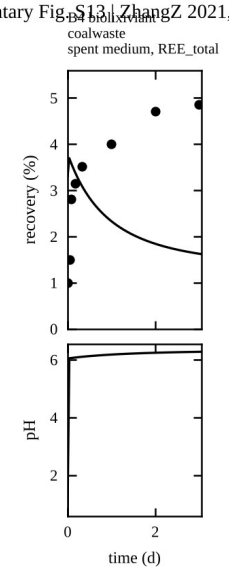
Supplementary Fig. S11. Zhang et al. (2022): fitted development runs. Each panel pair is one series, recovery above and pH below. Lines, model; symbols, measured.

Supplementary Fig. S12 | ZhangJ 2024, phosphogypsum. Each panel pair is one run: recovery above, pH below. Lines: fitted model; symbols: measured.



Supplementary Fig. S12. Zhang et al. (2024): fitted development runs. Each panel pair is one series, recovery above and pH below. Lines, model; symbols, measured.

Supplementary Fig. S13 | ZhangZ 2021, coal waste. Each panel pair is one run: recovery above, pH below. Lines: fitted model; symbols: measured.



Supplementary Fig. S13. Zhang et al. (2021): fitted development runs. Each panel pair is one series, recovery above and pH below. Lines, model; symbols, measured.